Enhanced STAT5a activation rewires exhausted CD8 T cells during chronic stimulation to acquire a hybrid durable effector like state

Jean-Christophe Beltra[1,2,3], Mohamed S. Abdel-Hakeem[1,2,4,5], Sasikanth Manne[1,2], Zhen Zhang[6], Hua Huang[6], Makoto Kurachi[7], Leon Su[8], Lora Picton[8], Yuki Muroyama[1,2], Valentina Casella[9], Yinghui J. Huang[1,2], Josephine R. Giles[1,2,3], Divij Mathew[1,2], Jonathan Belman[1,2], Max Klapholz[1,2], Hélène Decaluwe[10], Alexander C. Huang[2,3,11,12], Shelley L. Berger[6], K. Christopher Garcia[8,13,14,15] and E. John Wherry[1,2,3,16]

[1]Department of Systems Pharmacology and Translational Therapeutics, University of Pennsylvania, PA, USA
[2]Institute for Immunology, Perelman School of Medicine, University of Pennsylvania, Philadelphia, PA, USA
[3]Parker Institute for Cancer Immunotherapy at University of Pennsylvania, Philadelphia, PA, USA
[4]Department of Microbiology and Immunology, Faculty of Pharmacy, Cairo University, Kasr El-Aini, Cairo 11562, Egypt
[5]Current address: Department of Pathology and Laboratory Medicine, Emory University School of Medicine, Atlanta, GA, USA
[6]Department of Cell and Developmental Biology, Penn Institute of Epigenetics, Perelman School of Medicine, Philadelphia, PA 19104, USA
[7]Department of Molecular Genetics, Graduate School of Medical Sciences, Kanazawa University, Kanazawa 920-8640, Japan
[8]Departments of Molecular and Cellular Physiology and Structural Biology, Stanford University School of Medicine, Stanford, CA 94305, USA
[9]Infection Biology Laboratory, Department of Medicine and Life Sciences, Universitat Pompeu Fabra, Barcelona, Spain
[10]Cytokines and Adaptive Immunity Laboratory, Sainte-Justine University Hospital Research Center, Montreal, Quebec, Canada; Department of Microbiology and Immunology, Faculty of Medicine, University of Montreal, Montreal, Quebec, Canada; Immunology and Rheumatology Division, Department of Pediatrics, Faculty of Medicine, University of Montreal, Montreal, Quebec, Canada
[11]Department of Medicine, Perelman School of Medicine, University of Pennsylvania, Philadelphia, Pennsylvania 19104, USA
[12]Abramson Cancer Center, Perelman School of Medicine, University of Pennsylvania, PA, USA
[13]Stanford Cancer Institute, Stanford University School of Medicine, Stanford, CA 94305, USA.
[14]Parker Institute for Cancer Immunotherapy, 1 Letterman Drive, Suite D3500, San Francisco, CA 94129, USA.
[15]Howard Hughes Medical Institute, Stanford University School of Medicine, Stanford, CA 94305, USA
[16]Lead contact

*Correspondence: wherry@pennmedicine.upenn.edu

Abstract

Rewiring exhausted CD8 T cells (T_{EX}) towards more functional states is a major goal of cancer immunotherapy but has proven challenging due to the epigenetic stability of T_{EX}. Indeed, T_{EX} are epigenetically programmed by the transcription factor Tox. However, epigenetic changes continue to occur as T_{EX} transition from progenitor (T_{EX}^{prog}), to intermediate (T_{EX}^{int}) and terminal (T_{EX}^{term}) subsets, suggesting potential developmental flexibility in mature T_{EX} subsets. By examining the transition of T_{EX}^{prog} into T_{EX}^{int} cells, we discovered a reciprocally antagonistic circuit between Stat5a and Tox in T_{EX} cells. Stat5-activity controlled T_{EX}^{int} development, antagonized Tox, and instigated partial effector biology. Stat5 was also essential for T_{EX} reinvigoration by PD-1 blockade. Indeed, temporal induction of Stat5-activity in T_{EX} using an orthogonal IL-2/IL2Rβ-pair fostered T_{EX}^{int} cell accumulation and synergized with PD-L1 blockade. Constitutive Stat5a activity (STAT5CA) antagonized Tox-dependent T_{EX} epigenetic programming to generate a durable hybrid effector/NK-like population with enhanced tumor control. Finally, enforcing Stat5-signals in established T_{EX}^{prog} partially rewired the T_{EX} epigenetic landscape towards the effector/memory lineage. Together, these data highlight therapeutic opportunities of manipulating Stat5 to rewire T_{EX} towards a durably protective hybrid program.

(182 words)

Key words: CD8 T cell exhaustion, Stat5, epigenetic reprogramming, Tox, PD-1 blockade, T_{EX} intermediate, IL-2, orthogonal IL-2.

INTRODUCTION

CD8 T cell exhaustion is a common feature of chronic viral infections and cancers and limits effective control of disease[1,2]. T cell exhaustion is also a major barrier to effective immunotherapy for cancer including engineered cellular therapies[3] and has been implicated in autoimmune diseases.[2] First described as loss of effector functions in settings of chronic antigenic stimulation,[4,5] it is now clear that CD8 T cell exhaustion is a distinct epigenetically programmed state of T cell differentiation initiated by the HMG-transcription factor (TF) Tox.[6-10] This Tox-dependent epigenetic program also precludes (re)differentiation of T_{EX} towards functional effector (T_{EFF}) or memory (T_{MEM}) CD8 T cells.[11-14] Despite this altered differentiation state, T_{EX} acquire the unique ability to persist long-term despite chronic antigenic stimulation,[14,15] and exert partial control of chronic infections and cancer.[1,16-18] Moreover, relieving some inhibition of T_{EX} through PD-1 pathway blockade results in considerable clinical efficacy for some cancers.[19-24] Nevertheless, PD-1 pathway blockade fails to induce permanent epigenetic rewiring of T_{EX}[25,26] highlighting the need to identify strategies that can relieve the constraints on (re)differentiation of T_{EX} cells and allow conversion to more durably functional CD8 T cell states.

Recent work examining the developmental biology of T_{EX} cells has defined biologically distinct subsets that are related in a developmental hierarchy.[27-30] Molecular characterization of T_{EX} subsets has provided insights into subset-specific biology and their therapeutic relevance. For example, a Tcf1 (*Tcf7*)-expressing progenitor (T_{EX}^{prog}) subset retains proliferative potential and generates downstream T_{EX} subsets in the steady

state.[27,31-33] These T_{EX}^{prog} exist in two interchangeable states including a stem-like - quiescent subset (T_{EX}^{prog1}) that resides in lymphoid tissues and a transcriptionally distinct subpopulation (T_{EX}^{prog2}) that leaves these lymphoid niches and re-enters cell cycle. As these T_{EX}^{prog2} cells proliferate, they lose Tcf1 expression and differentiate into an intermediate "effector-like" subset (T_{EX}^{int}) that circulates in blood and ultimately converts to terminally exhausted CD8 T cells (T_{EX}^{term}) upon entering peripheral tissues where these T_{EX}^{term} also acquire features of tissue residency.[27] An additional set of insights involves the T_{EX}^{int} subset. First, PD-1 blockade functions as a transient amplifier of this T_{EX}^{int} population.[27,28] Although T_{EX}^{prog} initiate the proliferative response to PD-1 blockade,[31,32] subsequent production of new "effector-like" T_{EX}^{int} cells likely mediates the therapeutic benefits. Second, partial re-acquisition of effector features by T_{EX}^{int} cells in the landscape of a Tox-dependent exhaustion program suggests possible developmental flexibility. The molecular mechanisms of this potential T_{EX} rewiring, however, remain poorly understood. Thus, identifying mechanisms controlling T_{EX} subset conversions and biology, particularly at the T_{EX}^{int} stage could reveal opportunities to rewire the differentiation trajectory of T_{EX} for therapeutic benefit.

Here, we discovered a reciprocal antagonistic circuit between Tox and Stat5a in T_{EX} including preferential re-engagement of Stat5a activity in the T_{EX}^{int} subset. Indeed, Stat5 was essential for T_{EX}^{int} cell development as well as for the response to PD-1 pathway blockade. Moreover, Stat5 controlled re-activation of effector-like machinery acquired at the T_{EX}^{int} stage, fostering cytolytic effector functions even in the context of a T_{EX} chromatin landscape. Enforcing constitutive Stat5a activity (STAT5CA) antagonized Tox and the

Tox-dependent T_{EX} programing in chronic viral infection. This enforced Stat5a activity resulted in the induction of a suite of effector and NK-like biology in virus-specific CD8 T cells. These changes were driven by re-wired epigenetic and transcriptional circuitry and resulted in durable accumulation, and superior protective capacity, of STAT5CA-expressing CD8 T cells in settings of chronic viral infection and cancer. Therapeutic delivery of IL-2/Stat5-signals selectively to T_{EX} cells using an orthogonal IL-2/IL2Rβ pair system enhanced formation of T_{EX}^{int} cells and synergized robustly with PD-1 blockade. Finally, temporal reactivation of Stat5 in T_{EX}^{prog} reversed key epigenetic features of exhaustion, restored accessibility at T_{EFF}/T_{MEM}-related open chromatin regions and improved polyfunctionality. Together, these observations identify Stat5 as a key regulator of T_{EX} differentiation, antagonizing Tox-driven terminal exhaustion and fostering improved effector activity and durability in the setting of chronic antigen (Ag) stimulation. Moreover, accessing this biology by therapeutic augmenting Stat5 signals specifically in T_{EX} in combination with PD-1 blockade not only expanded the T_{EX}^{int} population but also rewired these T_{EX} cells towards a more protective differentiation state with features of durability under chronic antigenic stress and enhanced effector biology.

Results

Tox restrains Stat5a activity in virus-specific CD8 T cells during chronic infection

During chronic viral infections and cancer, Tox fosters epigenetic commitment of Ag-specific CD8 T cells towards exhaustion.[6-9] This fate commitment to T_{EX} is mediated in part by antagonizing pathways of functional effector (T_{EFF}) and memory (T_{MEM}) cell differentiation. However, partial transcriptional and epigenetic re-engagement of effector biology occurs at the T_{EX}^{int} cell stage suggesting the existence of yet unidentified pro-effector molecular circuits capable of temporally counterbalancing the Tox-dependent exhaustion program.[27] To identify potential mechanisms of re-engagement of effector circuitry in T_{EX} cells, we investigated transcriptional circuits and upstream regulators preferentially antagonized by Tox in virus-specific CD8 T cells during chronic viral infection. We performed Ingenuity Pathways Analysis (IPA) on differentially expressed genes (DEGs) between WT and Tox-deficient TCR transgenic "P14" CD8 T cells specific for LCMV D^bgp_{33-41} from previously published RNA sequencing (RNAseq) data (**Fig. S1A**).[7] Networks of transcriptional regulators involved in interferon signaling (i.e. *Irf1*, *Irf7*, *Stat1*) and terminal exhaustion (i.e. *Foxo1*) enriched in WT P14 cells. Conversely, TFs associated with T_{EFF} or T_{MEM} differentiation (i.e. *Tbx21*, *Id3* and *Stat5a*) had elevated transcriptional activity in Tox-deficient P14 cells (**Fig. S1B, Table S1**). Using a second single cell RNA sequencing (scRNAseq) dataset,[6] transcriptional networks of Tbet and Stat5a again enriched in Tox-deficient compared to WT D^bgp33^+ CD8 T cells and these TFs scored among the top 10 regulators enriched in 3 out of the 5 main clusters of cells identified (**Fig. S1C-G, Table S1**). Among the transcriptional regulators identified by IPA, Tbet and Stat5a overlapped with a list of TFs independently predicted using Taiji

142 analysis[34] to selectively impact T_{EX}^{int} cells compared to other T_{EX} subsets (**Fig. S1H**).[27]
143 Previous work identified bi-directional antagonism between Tbet and Tox in T_{EX}^{int} cells.[27]
144 However, Taiji analysis predicted Stat5a activity to be even more specifically enriched in
145 the T_{EX}^{int} subset than Tbet, and the IPA-defined transcriptional network of Stat5a was
146 more strongly anti-correlated with Tox expression than Tbet (**Fig. 1A** and **S1H).** These
147 analyses suggested a possible antagonistic axis between Tox and Stat5a in T_{EX} cells.
148 Indeed, the transcriptional signatures of Stat5a and Tox were inversely correlated in Ag-
149 specific CD8 T cells at 1 week and 1 month of chronic infection (**Fig. 1B-C**). Stat5a activity
150 in T_{EX} cells was also anti-correlated with the expression of exhaustion-specific genes, but
151 positively associated with genes involved in effector-related biology (**Fig. S1I**). These data
152 suggested a role for Stat5a in antagonizing Tox and the program of CD8 T cell exhaustion.
153
154 **STAT5a reduces Tox expression, antagonizes exhaustion and fosters effector-like**
155 **CD8 T cell differentiation during chronic viral infection**
156 During the first week of a developing chronic viral infection, Ag-specific CD8 T cells
157 differentiate into either effector-like CD8 T cells or precursors of T_{EX}.[26,35] Because the
158 potential Stat5a and Tox antagonism observed above was evident by d8p.i., we asked
159 whether Stat5a could impact early CD8 T cell-fate commitment during chronic infection.
160 Congenically distinct P14 cells were transduced with retroviruses (RV) encoding either a
161 constitutively active form of Stat5a (P14 STAT5CA)[36,37] or a control RV (P14 Empty). RV-
162 transduced P14 cells were sort-purified based on RV-encoded reporter protein
163 expression (violet-excited [VEX] or green fluorescent protein [GFP]), mixed at a 1:1 ratio
164 and co-transferred into congenically distinct LCMV clone 13 (Cl13) infected mice (**Fig.**

2A). On d8p.i., expression of Tcf1 (or Ly108) and Tim3 can identify T_{EX} precursors (T_{EX}^{prec}; Tcf1/Ly108^{+}Tim3^{-}) or more differentiated "effector-like" CD8 T cells (Tcf1/Ly108^{-} Tim3^{+}) (**Fig. S2A**).[33,35] Both d8 populations were detected for P14 Empty controls. In contrast, most of the P14 STAT5CA cells (91.7±0.98%) had differentiated into Ly108^{-} Tim-3^{+} CD8 T cells whereas the Ly108^{+}Tim-3^{-} T_{EX}^{prec} population was substantially reduced in both frequency (2.7±0.4%) and absolute number for the STAT5CA RV group (4.3-fold lower numbers than the Empty RV group) (**Fig. 2B** and **S2B**). We further confirmed the decrease in the generation of T_{EX}^{prec} cells in P14 STAT5CA cells using unbiased clustering based on 12 flow cytometry parameters (**Fig. 2C**-see methods) or Tcf1 expression (**Fig. 2D**-upper panel). The overall numerical advantage of P14 STAT5CA cells over the P14 Empty at this early time-point (**Fig. S2B**) suggested a differentiation bias towards the Ly108^{-}Tim-3^{+} effector-like population at the expense of T_{EX}^{prec}. Enforcing Stat5a activity also resulted in substantially lower Tox expression (**Fig. 2D-**lower panel). At this early time point, production of antiviral cytokines by P14 Empty and P14 STAT5CA cells after gp33 peptide stimulation was similar (**Fig. S2C**). Expression of the inhibitory receptors (IR) PD-1, Lag-3, and Tigit was also equivalent between STAT5CA and Empty RV P14 cells whereas other IRs (2B4, Tim-3) and some effector-related molecules (Cx3cr1, Granzyme B [GzmB]) were more highly expressed by the STAT5CA P14 cells (**Fig. 2E**). Thus, during the first week of a chronic viral infection, increasing STAT5a activity reduced Tox expression and enhanced the development of Ly108^{-}Tim-3^{+} effector-like cells at the expense of T_{EX}^{prec}.

Stat5 supports early expansion of Ag-specific CD8 T cells in acutely resolving infections, though Stat5 activity in these settings has minimal impact on the balance of KLRG1$^+$ terminal T_{EFF} and CD127$^+$ memory precursors CD8 T cells.[38,39] To interrogate how Stat5 regulates differentiation of Ag-specific CD8 T cells early during chronic viral infection, naïve P14 WT (Rosa^{YFP}*Stat5a/b*$^{+/+}$) and P14 Stat5iKO (Rosa^{YFP}*Stat5a/b*$^{fl/fl}$) were treated with tat-cre recombinase *in vitro* (cre$^+$; or not [cre$^-$]) to induce genetic deletion of *floxed* alleles (**Fig. S2D**). Induction of YFP served as a surrogate for efficient cre-mediated recombination. We then adoptively transferred cre treated (cre$^+$) P14 WT or P14 Stat5iKO cells (or their cre$^-$ controls) into congenically distinct recipient mice that were infected with LCMV Cl13 and assessed the impact of loss of *Stat5a/b* at d8p.i. Genetic deletion of *Stat5a/b* resulted in a higher proportion of T_{EX}^{prec} cells and a reduction in Ly108$^-$Tim-3$^+$ effector-like cells (11±1% vs 47±2% and 85±1% vs 49±2% of T_{EX}^{prec} and Ly108$^-$Tim-3$^+$ cells in P14 WT vs P14 Stat5iKO respectively) (**Fig. 2F** and **S2E-F**). The overall number of P14 cells was reduced by ~11-fold in the absence of *Stat5a/b* but this effect was predominantly in the Ly108$^-$Tim-3$^+$ population that was reduced ~18-fold compared to the WT P14 cells (**Fig. 2G**). In contrast, the Ly108$^+$Tim-3$^-$ T_{EX}^{prec} were impacted less with only a ~2.7-fold reduction in the absence of *Stat5a/b*. Changes in proliferation or cell death did not appear to explain these differences between the WT and *Stat5a/b* iKO cells because BrdU incorporation (d7-8) and active caspase 3 were similar between these populations (**Fig. S2G-H**). These data suggested an impact on differentiation and in particular, an altered formation of Ly108$^-$Tim-3$^+$ cells in the absence of *Stat5a/b*, consistent with the enhanced development of this effector-like population using STAT5CA (**Fig. 2B**). This effect of *Stat5a/b*-deficiency appeared to be preferential to chronic

infection because, consistent with previous studies,[38,39] there was little impact of loss of *Stat5a/b* on the distribution of memory precursor and short-lived effector CD8 T cell subsets during acute LCMV Armstrong (Arm) infection (**Fig. S2I**). Consistent with the reduction of Tox upon constitutive activation of Stat5a (**Fig. 2D**), loss of *Stat5a/b* resulted in increased Tox expression in P14 Stat5iKO compared to P14 WT during Cl13 infection (**Fig. 2H**). The minimal role of Tox at early stages of acutely resolving versus chronic infection[6,7] may explain the preferential impact of Stat5 during LCMV Cl13 infection compared to Arm infection. Moreover, these data indicate a role for Stat5 in the early population dynamics during evolving chronic infection with Stat5 activity repressing Tox and fostering differentiation into the more effector-like Ly108^{-}Tim-3^{+} subset during the first week of infection.

Constitutive STAT5a activation promotes an epigenetic state with features of effector and exhausted CD8 T cells during chronic infection

Commitment of CD8 T cells to exhaustion is associated with acquisition of a distinct epigenetic landscape.[6,26,40] To investigate whether constitutively active Stat5a altered early epigenetic programming of Ag-specific CD8 T cells, we performed Assay for Transposase-Accessible Chromatin followed by high throughput sequencing (ATACseq)[41] on P14 Empty and P14 STAT5CA cells at d8 of Cl13 infection and compared these data to P14 cells isolated at d8 of Arm infection (T_{EFF}). Examining all differentially accessible peaks (DAPs; lfc>2, FDR≤0.01), each population of P14 cells was distinct in principal component space (**Fig. 3A**) or by Spearman distance analysis (**Fig. S3A**) with P14 Empty and P14 STAT5CA differing from each other by almost the same “distance”

as they each differed from the T_{EFF} cells from Arm infection. Indeed, P14 Empty and P14 STAT5CA differed from Arm-derived T_{EFF} by 27,876 and 25,681 DAPs respectively. P14 STAT5CA cells also differed from their P14 Empty controls in chronic infection by 16,901 DAPs (**Fig. 3B, Table S2**). The majority of DAP were at intergenic, promoter and intronic regions (**Fig. S3B**). One possible explanation for these epigenetic differences could be the near absence of the Ly108^{+}Tcf1^{+} T_{EX}^{prec} population in P14 STAT5CA (**Fig. 2B**) and subsequent absence of the Tcf1 signature. However, of the 16,901 DAPs between P14 Empty and P14 STAT5CA cells, only 454 peaks (2.7%) related to genes differentially expressed between WT and *Tcf7*$^{-/-}$ gp33^{+} CD8 T cells from d7 post LCMV Cl13 infection (**Fig. S3C)**.[33] This observation suggested that the distinct ATAC profile of P14 STAT5CA cells was not simply due to the absence of Tcf1-expressing T_{EX}^{prec} cells in this population, but rather reflected epigenetic remodeling provoked by constitutive Stat5a expression.

To examine how constitutive Stat5 expression impacted the early establishment of exhaustion in Ag-specific CD8 T cells, we performed K-means clustering of the 16,901 DAPs between P14 Empty and P14 STAT5CA (**Fig. 3C, Table S2**). Cluster 1 and 4 (C1,-4) contained regions preferentially remodeled in P14 STAT5CA cells. In contrast, C2, -3 and -5 contained DAPs with selectively increased or decreased accessibility in P14 Empty cells but the opposite trend in both P14 STAT5CA and T_{EFF} cells (**Fig. 3C**). Hence, among the 16,901 DAPs between P14 Empty and P14 STAT5CA cells, 62% (10,445 peaks; [C2,-3 and-5]) represented changes in which P14 STAT5CA cells became more similar to T_{EFF} compared to P14 Empty cells. DAPs in C1 (gained in P14 STAT5CA) strongly enriched for Stat5 binding motifs (also potentially bound by Stat1, -3 and -4) and motifs for effector-

related TFs (Runx1/2) (**Fig. 3C-D**; **Table S2**). C4 DAPs (decreased in P14 STAT5CA) rather contained T-box and homeobox TFs motifs (i.e. Eomes, T-bet, Tbr1, Tbx2-6, Tgif1/2). C2 with high accessibility in P14 Empty was enriched in binding motifs for TCR-dependent TFs with established roles in T_{EX} including NFAT (RHD) and BATF (bZIP) and this cluster included open chromatin regions at exhaustion-specific genes (i.e. *Tox*, *Tox2*) (**Fig. 3C-D** and **S3D**). C3 and -5 with increased accessibility in both P14 STAT5CA and T_{EFF} compared to P14 Empty, contained several DAPs located near genes encoding effector-related molecules and TFs (i.e. *Gzma*, *Fasl*, *Prf1*, *Runx1/3*, *Id2*) and enriched for Stat5, Runx1/2 and ETS motifs (**Fig. 3C-D** and **S3D**). Further clustering of all DAPs between P14 Empty, P14 STAT5CA and T_{EFF} (70,458 peaks) revealed decreased accessibility at a large fraction of exhaustion-related open chromatin regions in P14 STAT5CA cells concomitant with a shift to a more effector-like open chromatin landscape (**Fig. S3E**). Together, these data highlight an altered epigenetic program in P14 STAT5CA cells early during chronic viral infection and shift towards effector biology at the stage of differentiation when epigenetic imprinting of exhaustion typically occurs.

Consistent with this antagonism of the early program of exhaustion, a large fraction of open chromatin regions near Tox-dependent or exhaustion-related genes were lost in P14 STAT5CA cells, whereas accessibility at effector-associated genes was increased (**Fig. 3E**). A substantial proportion of genes from these core signature lists possessed one or several Stat5 binding sites, suggesting direct regulation of genes involved in effector versus exhaustion biology by this TF (**Fig. 3F**, **Table S2**). *Tox* was among the top exhaustion-related genes with reduced chromatin accessibility in P14 STAT5CA

compared to P14 Empty cells consistent with lower expression of Tox in the former population (**Fig. 2D**). Moreover, this gene contained one of the highest numbers of direct Stat5 binding sites (**Fig. 3G**)**.** To explore the relationship between Tox and Stat5a, we further analyzed the *Tox* locus (**Fig. 3H**). Overall, chromatin accessibility decreased in *Tox* in P14 STAT5CA compared to P14 Empty cells, notably at enhancers in the first intron (**Fig. 3H-I**). Indeed, accessibility at one region in the first intron was decreased to a level comparable to or even lower than that observed in T_{EFF} cells (**Fig. 3I**). This region was also enriched for active H3K27Ac histone marks, particularly in settings of chronic Ag-stimulation (P14 Empty Cl13 D8) suggesting an active chromatin environment in early T_{EX} (**Fig 3H**). Indeed, this region contained, and was framed by several binding sites for NFAT1[42] and NFAT2[43] (**Fig. 3H,J**), TFs that are key drivers of Tox induction during the early development of T_{EX}.[6,7,10] This active H3K27Ac chromatin environment in intron 1 was reduced in P14 STAT5CA cells suggesting that enforced STAT5 activity impedes chromatin accessibility in *Tox*, particularly at sites where the transcriptional drivers of Tox induction (NFATs) can bind. Together, these data highlight the potential impact of Stat5 in the epigenetic regulation of key exhaustion-related genes including *Tox* where Stat5 appears to function directly to modulate accessibility in this locus at locations where NFAT proteins may act.

Constitutive STAT5a activation instigates a distinct effector/NK-like transcriptional program and improves therapeutic potential

Establishment of a Tox-dependent exhaustion program drives altered function, but also is required for the maintenance of T_{EX} during chronic infections and cancer.[6-9,31,32] Without

Tox, T_{EX} cannot form or persist in the setting of chronic Ag stimulation. Because constitutive Stat5a activation antagonized Tox, we next investigated the durability and fate of P14 STAT5CA cells later during chronic viral infection. We again employed the co-adoptive transfer model where P14 Empty and P14 STAT5CA cells could be examined in the same chronically infected recipient mice. At d27p.i., 85±4.5% of the RV transduced (VEX^+) donor P14 cells were P14 STAT5CA cells and this population numerically outcompeted their P14 Empty counterpart in the spleen as well as peripheral tissues (**Fig. 4A-B** and **S4A-C**). This numerical advantage of P14 STAT5CA cells was also observed even in mice with life-long viremia due to transient depletion of CD4 T cells (Cl13 αCD4; **Fig. 4A**-right) where cells persisted for at least ~3 months (**Fig. S4D**) suggesting a prolonged advantage of this enforced STAT5CA expression. At d27p.i., the donor P14 STAT5CA population was enriched for $Ly108^-CD69^-$ T_{EX}^{int} cells. The proportion of the two $Tcf1^+$ progenitor subsets, T_{EX}^{prog1} ($Ly108^+CD69^+$) and T_{EX}^{prog2} ($Ly108^+CD69^-$) were dramatically reduced, though a small population of the latter was present, and the frequency of T_{EX}^{term} ($Ly108^-CD69^+$) was also reduced compared to the P14 Empty population from the same mice (**Fig. 4C** and **S4E**). Thus, constitutive Stat5a activation leads to an accumulation advantage for virus-specific CD8 T cells in the setting of a chronic viral infection, despite the substantial reduction in $Tcf1^+$ T_{EX}^{prog} cells, mainly through an accumulation of T_{EX}^{int}-like cells.

Based on the ATAC-seq data from d8 p.i., we hypothesized that the P14 STAT5CA cells later in chronic infection might differ from previously defined T_{EX}^{int} despite their $Ly108^-$ $CD69^-$ phenotype. We therefore performed single-cell RNA sequencing (scRNA-seq) to

compare P14 STAT5CA and P14 Empty cells at ~1 month of chronic viral infection. We identified canonical clusters of T_{EX} cells including a T_{EX} progenitor cluster (C4; progenitors [T_{EX}^{prog}]) selectively expressing *Tcf7, Slamf6,* and *Xcl1* and two clusters that enriched for a signature of T_{EX}^{term} (C0 and C1) and expressed *Cxcr6*, a marker associated with terminal exhaustion[30] as well as elevated *Pdcd1*, *Cd160 and CD244* (2B4) (**Fig. 4D** and **S4F-G**). We also identified two clusters of *Cx3cr1*-expressing cells, one of which was consistent with T_{EX}^{int} cells (C3). A second cluster (C2; Effector/NK-like) also enriched for a T_{EX}^{int} cell signature but displayed selective expression of NK cell receptors (i.e. *Klre1*, *Klrk1*, *Klrd1*), elevated transcripts of effector molecules and TFs (i.e. *Gzma, Zeb2*) (**Fig. 4D** and **S4F-G, Table S3**), similar to a recently described NK-like T_{EX} subset.[26,44] This subset also had reduced expression of several exhaustion-related genes including *Tox* and *Pdcd1* compared to all other clusters (**Fig. 4D** and **S4F-G, Table S3**). This effector/NK-like cluster (C2) was composed mostly of P14 STAT5CA cells with little contribution of P14 Empty cells. Rather, the latter were more evenly distributed throughout C0,1,3, and -4 (**Fig. 4E** and **S4H**). Consistent with the high expression of NK- and effector-genes in C2, these cells also enriched for the transcriptional signatures of short-lived effector CD8 T cells (SLEC) and had the lowest enrichment score for an exhaustion or Tox-dependent transcriptional signature among clusters of CD8 T cells from Cl13 infection (**Fig. 4F**). Moreover, although the P14 STAT5CA cluster (C2) mapped closely to the T_{EX}^{int} cluster (C3) in a UMAP representation (**Fig. 4D**), these two clusters differed by expression of 211 genes (Log2FC>0.5, p_value_adj≤0.05) with T_{EX}^{int} cells mostly composed of P14 Empty cells having higher expression of exhaustion-related genes including *Tox*, *Eomes*, *Pdcd1, Lag3* whereas the P14 STAT5CA cells had higher

expression of genes encoding effector or NK cell-related markers (e.g. *Klre1, Klrb1c, Klrk1, Klrd1*, *Gzma, Tbx21*), and genes involved in cell survival (e.g. *Bcl2)* (**Fig. 4G-H, Table S3**). Lastly, genes with increased chromatin accessibility in P14 STAT5CA cells at d8p.i. (**Fig. 3, Table S4**) had higher mRNA expression in P14 STAT5CA cells (C2) at d27p.i. (**Fig. 4I**), suggesting that the transcriptional differences observed in P14 STAT5CA cells at d27p.i. reflected, at least in part, the chromatin accessibility landscape established by d8 p.i. Together these data suggested that constitutive STAT5a activation drove virus-specific CD8 T cells into a distinct state during chronic infection characterized by a transcriptional program with both effector and NK-like features in this setting that typically drives CD8 T cell exhaustion.

The enhanced effector/NK biology of P14 STAT5CA cells coupled with the accumulation advantage in chronic infection prompted us to evaluate disease control and/or therapeutic efficacy. Because during LCMV Cl13 infection even small changes in the number of WT P14 alter pathogenesis[45,46] complicating questions of protective immunity, we used a tumor model where the ability to control tumor growth could be assessed. P14 STAT5CA and P14 Empty cells were adoptively transferred separately into mice with established B16-gp_{33-41} tumors (d10 post tumor inoculation) (**Fig. 4J**). Adoptive transfer of P14 Empty cells into these mice only slightly delayed tumor growth whereas P14 STAT5CA cells resulted in substantial reduction in tumor burden and survival of all mice in this group (**Fig. 4K-L**). Thus, the impact of constitutively active STAT5a on differentiation of CD8 T cells not only antagonized exhaustion, but these changes in CD8 T cell differentiation corresponded to improved therapeutic efficacy and control of tumor growth.

STAT5 is essential for generation of T_{EX}^{int} cells and for response to PD-L1 blockade

We next used the adoptive transfer approach to investigate how endogenous Stat5 influenced T_{EX} dynamics when exhaustion was fully established using P14 WT and P14 Stat5iKO cells (**Fig. S2D**). At ~1 month p.i., P14 Stat5iKO cells had high expression PD-1 and Tox (albeit slightly reduced compared to P14 WT) but lacked expression of molecules associated with T_{EX}^{int} or T_{EX}^{term} (i.e. Granzyme B, Cx3cr1, Tim-3; **Fig. 5A**). Indeed, the P14 Stat5iKO population was almost exclusively composed of T_{EX} progenitors (T_{EX}^{prog1} and T_{EX}^{prog2}) with only minor populations of T_{EX}^{int} cells and T_{EX}^{term} compared to P14 WT cells or STAT5-proficient (cre-/YFP-) controls from the same donor P14 population (**Fig. 5B** and **Fig. S5A-B**). As a result, the number of P14 Stat5iKO cells in the spleen was reduced compared to P14 WT cells with even more substantial reductions in the blood and peripheral tissues consistent with the accumulation of T_{EX}^{int} and T_{EX}^{term} cells in these locations (**Fig. 5C** and **S5C-D**).[27] However, the T_{EX}^{prog1} and T_{EX}^{prog2} compartments remained numerically intact in the absence of *Stat5a/b* (**Fig. 5C**). The stability of these progenitor-like CD8 T cells in chronic viral infection in the absence of *Stat5a/b* was in stark contrast to the ~23-fold reduction in the number of memory CD8 T cells formed by P14 Stat5iKO following an acute infection with LCMV Arm (**Fig. 5D**) highlighting the distinct dependency on *Stat5a/b* for the formation and/or maintenance of T_{MEM} in acutely resolving versus T_{EX}^{prog} in chronic viral infection.

As T_{EX}^{prog1} cells exit quiescence, they convert to T_{EX}^{prog2} cells that re-engage cell-cycle and further differentiate into T_{EX}^{int} cells. This T_{EX}^{prog2} to T_{EX}^{int} transition is amplified by PD-1 pathway blockade.[27] In the absence of *Stat5a/b*, proliferation of T_{EX}^{prog1} and T_{EX}^{prog2} was

reduced compared to P14 WT (**Fig. S5E**). This reduced proliferation suggested a defect in the conversion of T_{EX}^{prog1} and T_{EX}^{prog2} into T_{EX}^{int} cells without *Stat5a/b*. PD-L1 blockade did not rescue the development of T_{EX}^{int} cells for P14 Stat5iKO cells and these cells failed to expand in number following PD-L1 blockade despite a numerically intact progenitor compartment (**Fig. 5E** and **S5F-G**). Thus, Stat5 was essential for proliferation-driven conversion of T_{EX}^{prog1} and T_{EX}^{prog2} into T_{EX}^{int}, a key developmental transition for generation of more terminally differentiated T_{EX} subsets, replenishment of peripheral immunity and response to PD-1 blockade.

To investigate the molecular effects of Stat5-deficiency in T_{EX} subsets, we performed Cellular Indexing of Transcriptomes and Epitopes by sequencing (CITE-seq) on P14 WT and P14 Stat5iKO cells at ~1 month of chronic infection. Using RNA-based unsupervised clustering, we again identified major clusters of T_{EX} cells and confirmed the near absence and robust reduction of the T_{EX}^{int} and T_{EX}^{term} subsets respectively in P14 Stat5iKO compared to P14 WT (**Fig. 5F,G** and **S6A,B**). Top DEGs between WT and Stat5iKO P14 cells reflected this altered subset distribution with increased expression of progenitor-associated genes (i.e. *Tcf7*, *Id3*, *Xcl1*) but depletion of genes related to more differentiated subsets (i.e. *Cx3cr1*, *Cxcr6*, *Gzma*, *Gzmb*) in the later population (**Fig. 5H, Table S5**). Comparing clusters also revealed transcriptional divergence between P14 Stat5iKO and P14 WT cells in the three main clusters, suggesting that STAT5-deficiency affected all major subsets of T_{EX} cells (**Fig. S6C**).

The T_{EX}^{prog1} and T_{EX}^{prog2} often co-segregate in scRNA-seq space because of the dominance of the progenitor signature. However, the T_{EX}^{prog2} subset engages distinct biology as these cells begin to downregulate *Tcf7*, enter cell cycle and initiate the transition to downstream T_{EX} subsets.[27] CITE-seq captured this key transitional biology by discriminating Ly108^{+}CD69^{-} T_{EX}^{prog2} cells using surface markers and allowed us to further interrogate Stat5a/b-dependent transcriptional differences in this subset (**Fig. S6D-F**). Indeed, analysis of DEGs confirmed transcriptional differences between oligo-tagged antibody-defined T_{EX} subsets (**Fig. 5I, Table S5**). Of interest, the Stat5-dependent cyclin *Ccnd2* that initiates the G1-S cell-cycle phase was elevated in all P14 WT T_{EX} subset compared to P14 Stat5iKO cells consistent with a defect in cell-cycle re-entry in the absence of *Stat5a/b* (**Fig. 5J**). This reduced *Ccnd2* expression was coupled with a robust decrease in expression of multiple genes encoding ribosomal proteins (*Rps* genes) in P14 Stat5iKO cells, particularly in T_{EX}^{prog1} and T_{EX}^{prog2} cells (**Fig. 5J**). This observation suggested a reduction in protein synthesis in *Stat5a/b*-deficient T_{EX} coupled to a defect in differentiation potential. *Stat5a/b*-deficient T_{EX}^{prog2} cells also retained higher expression of progenitor associated-molecules (i.e. *Tcf7*, *Sell*, *Slamf6*, *Id3*, *Tox*) whereas these genes are typically reduced during the T_{EX}^{prog1} to T_{EX}^{prog2} transition.[27] Expression of some of these progenitor-related molecules even trended higher in the few *Stat5a/b*-deficient T_{EX}^{int} and T_{EX}^{term} cells detectable (e.g. *Sell*, *Slamf6*, *Tcf7*, *Tox*) compared to P14 WT T_{EX}^{int} and T_{EX}^{term} cells (**Fig. 5J**). In addition, the few T_{EX}^{int} cells that developed in the absence of *Stat5a/b* had impaired expression key effector genes including (i.e. *Gzma*, *GzmB*, *Cx3cr1*, *Zeb2*, *Tbx21*, *Id2*) and multiple KLR-molecules (i.e. *Klrd1*, *Klre1*, *Klrc1*, *Klrc2*, *Klrk1*), though because of the small number of Stat5iKO T_{EX}^{int} cells, many of these

changes did not reach statistical significance. However, this lack of effector-biology in P14 Stat5iKO T_{EX}^{int} cells was also apparent at the T_{EX}^{term} stage (i.e. reduced *Gzmb*, *Gzma*) and these cells also had reduced expression of *Bcl2* perhaps contributing to poor survival in the absence of *Stat5a/b* (**Fig. 5J**). Together, these data point to a key inability of T_{EX}^{prog2} cells to exit quiescence, re-engage cell-cycle and engage the transition to the T_{EX}^{int} stage in the absence of *Stat5a/b*. Stat5 also mediated the transcriptional switch that accompanied this T_{EX}^{prog2}-to-T_{EX}^{int} transition by extinguishing at least some of the T_{EX} progenitor-associated biology and fostering the effector and NK-like features that characterize the T_{EX}^{int} subset.

Temporal reactivation of Stat5 in T_{EX} cells drives T_{EX}^{int} cell accumulation and synergizes with PD-L1 blockade

Given the key role of Stat5 for T_{EX}^{int} cell generation described above, we next explored the potential of temporally manipulating this axis to foster development of this subset. To this end, we leveraged an orthogonal IL-2/IL2Rβ system.[47] Briefly, P14 CD8 T cells were transduced with an RV encoding an orthogonal IL2Rβ-receptor chain (*ortho*IL2Rβ; P14 IL2Rβ-ortho) that selectively binds and triggers Stat5 activation in response to cognate orthogonal IL-2 (*ortho*IL-2) but not the native endogenous IL-2 and compared these cells to those transduced with an empty RV (P14 Empty). Congenically distinct P14 IL2Rβ-ortho and P14 Empty cells were co-transferred into mice infected with LCMV Cl13 (**Fig. 6A**). Starting on d21p.i., groups of mice received escalated doses of *ortho*IL-2 for 5 days and changes in total T_{EX} and T_{EX} subsets were examined at d26p.i. *In vivo* delivery of *ortho*IL-2 caused a selective and dose dependent expansion of the YFP^+ (RV^+) P14

462 IL2Rβ-ortho cells compared to their P14 Empty control counterparts (**Fig. 6B**). This dose-
463 dependent numerical increase was not observed in YFP$^-$ (RV$^-$) cells and, unlike WT IL-2,
464 *ortho*IL-2 treatment also did not alter the frequency of regulatory T cells, demonstrating
465 the specificity of the *ortho*IL-2/IL2Rβ system (**Fig S7A-B**). Moreover, although the
466 frequency of T_{EX} subsets remained similar in the P14 Empty population and endogenous
467 gp_{33-41}-specific CD8 T cells (**Fig. S7C-D**), the P14 IL2Rβ-ortho population in the same
468 mice displayed an expansion of T_{EX}^{prog2} and T_{EX}^{int} cells and concomitant reductions in the
469 frequency of T_{EX}^{prog1} and T_{EX}^{term} cells with increasing doses of *ortho*IL-2 in both the spleen
470 and peripheral tissues (**Fig. 6C-D** and **S7E-H**). The gradual decrease in T_{EX}^{term} cell
471 frequency within P14 IL2Rβ-ortho also suggested that *ortho*IL-2-mediated Stat5
472 activation stabilized the T_{EX}^{int} stage, restraining conversion to the more terminally
473 exhausted T_{EX}^{term} cells. Although the frequency of stem-like T_{EX}^{prog1} cells among the P14
474 IL2Rβ-ortho populations treated with *ortho*IL-2 decreased in a dose dependent manner,
475 the absolute number of these key progenitor cells remained stable (**Fig. S7I**) suggesting
476 that *ortho*IL-2 treatment could enhance the generation of downstream T_{EX} subsets without
477 depleting the T_{EX} progenitor populations. These data indicate that temporal engagement
478 of the *ortho*IL-2 system in T_{EX} cells, likely through increasing Stat5 activity, can function
479 as an amplifier of the T_{EX}^{prog2} transition into T_{EX}^{int} cells.
480
481 Because expansion of T_{EX}^{prog2} and T_{EX}^{int} cells is also observed following PD-1/PD-L1
482 pathway blockade,[27] we next tested the potential of PD-1 pathway blockade to combine
483 with *ortho*IL-2. P14 Empty and P14 IL2Rβ-ortho cells expanded similarly upon PD-L1
484 blockade. However, the P14 IL2Rβ-ortho cells substantially outnumbered their P14 Empty

485 counterpart in the same mice when *ortho*IL-2 was provided at the time of PD-L1 blockade
486 (**Fig. 6F-G** and **S7J-K**). This burst in P14 IL2Rβ-ortho cell number was due to a selective
487 amplification of T_{EX}^{prog2} and an even more robust increase in T_{EX}^{int} cells (**Fig. 6H-I**). Thus,
488 the strong combinatorial potential of IL-2-derived signals to synergize with PD-1/PD-L1
489 blockade reported previously[48] resides in the convergence of the two approaches at
490 amplifying the T_{EX}^{int} subset likely in a Stat5-dependent manner.
491
492 **Temporal reactivation of Stat5 in T_{EX} progenitors enables functional recovery and**
493 **partial epigenetic rewiring towards the T_{EFF}/T_{MEM} lineage upon rechallenge**
494 Given the ability of Stat5-dependent signals to restrain exhaustion and foster effector-like
495 biology, we next tested whether engaging Stat5 in combination with strong re-
496 differentiation signals could rewire the epigenetic program of mature T_{EX} cells. To test this
497 idea, we sort-purified RV transduced IL2Rβ-ortho Ly108$^+$ T_{EX} progenitors cells on d27p.i.,
498 after exhaustion was fully established (**Fig. S8A**). These cells were adoptively transferred
499 into congenic naïve recipient mice and these mice were subsequently challenged with
500 LCMV Arm to provide a strong (re)differentiation signal (**Fig. 7A**). On day 3-to-7 post
501 challenge (p.ch.), recipient mice received daily injections of PBS or *ortho*IL-2 (150KIU)
502 with or without anti-PD-L1 (**Fig. 7A**). We compared these responses to recall responses
503 of conventional memory P14 CD8 T cells (Memory; T_{MEM}) isolated from LCMV Arm mice
504 (d>90p.i.) (**Fig. 7A** and **S8A**). When compared head-to-head, T_{MEM} cells numerically
505 outperformed Ly108$^+$ T_{EX} progenitors from the PBS-treated group ($T_{EX}^{[PBS]}$) by ~54-fold
506 on d8 p.ch. (**Fig. 7B**), consistent with previous observations.[11] $T_{EX}^{[PBS]}$ also remained poor
507 cytokine producers, had lower expression of cytolytic molecules (i.e. Gzmb, Gzma),

rapidly re-expressed Tox and PD-1, and generated few KLRG1^{+}CD127^{-} secondary T_{EFF} compared to the donor T_{MEM} (**Fig. 7C-E**). In contrast, however, IL2Rβ-ortho Ly108^{+} T_{EX} progenitors treated with *ortho*IL-2 ($T_{EX}^{[oIL2]}$) during re-challenge underwent robust secondary expansion compared to their PBS-treated counterparts, approaching the expansion potential of T_{MEM} cells, especially when *ortho*IL-2 was combined with PD-L1 blockade (**Fig. 7B**). The accumulation advantage of $T_{EX}^{[oIL2]}$ cells versus $T_{EX}^{[PBS]}$ persisted at d40 p.ch. (**Fig. S8B**). *Ortho*IL-2 treatment was sufficient to restore polyfunctionality as assessed by IFNγ and TNF production and this polyfunctionality was not further enhanced by addition of PD-L1 blockade (**Fig. 7C**). *Ortho*IL-2 treatment also resulted in higher expression of effector related molecules reaching levels similar to (T-bet, CD94, GzmB) or even higher (GzmA) than observed for secondary T_{EFF} responses derived from T_{MEM} and those qualitative changes occurred in the absence of an increase in the KLRG1^{+} population (**Fig. 7D, E**). Tox expression was reduced in $T_{EX}^{[oIL2]}$ cells whereas PD-1 expression remained unchanged compared to the PBS treatment group (**Fig. 7D**), consistent with the additional benefit of blocking the PD-1 pathway in combination with *ortho*IL-2 treatment (**Fig. 7B** and **D**). Thus, in this rechallenge setting, *ortho*IL-2 treatment synergized with PD-L1 blockade for robust expansion of T_{EX} progenitor cells and accessing the IL-2-STAT5 axis in this setting had a selective qualitative impact on restoring robust expansion, polyfunctionality and effector biology.

To interrogate the mechanisms of this *ortho*IL-2 treatment benefit on T_{EX} cells, we performed ATAC-seq on T_{MEM}, $T_{EX}^{[PBS]}$ and $T_{EX}^{[oIL2]}$ at d8p.ch. Principle component analysis revealed distinct chromatin landscapes for T_{MEM}, $T_{EX}^{[PBS]}$ and $T_{EX}^{[oIL2]}$ with 4701

DAPs (lfc>2, FDR≤0.01) by pairwise comparisons (**Fig. 7F,G, Table S6**). K-means clustering of all DAPs identified modules of open chromatin regions preferentially accessible in cells originating from T_{EX}^{prog} (open in $T_{EX}^{[PBS]}$ vs T_{MEM}; C1 and C2; Exhaustion-Modules) or T_{MEM} cells (open in T_{MEM} vs $T_{EX}^{[PBS]}$; C3 and C4; Memory-Modules) (**Fig. 7H, Table S6**). These data indicated that even in settings of strong (de)differentiation signals, scars of the exhaustion epigenetic landscape persisted in cells that expanded from T_{EX}^{prog}.[11,13] Targeted delivery of *ortho*IL-2-signals, however, reversed parts of this epigenetic program in T_{EX}^{prog}-derived cells (**Fig. 7H**; C2; Exhaustion-module "Reversed") and even allowed for acquisition of open chromatin patterns associated with the T_{EFF}/T_{MEM} lineage (**Fig. 7H**; C4; Memory module "Reacquired"). In addition, *ortho*IL-2 treatment resulted in a selectively increased accessibility at a large fraction of chromatin regions that were otherwise closed in both $T_{EX}^{[PBS]}$ and T_{MEM}-derived cells (**Fig. 7H**; C5; "IL2-Stat5 module"). Notably, *ortho*IL-2 treatment increased chromatin accessibility at genes related to cell proliferation (*Cdkn2b*), effector differentiation (*Id2*, *Klrb1c*), IL-2/Stat5 responsiveness (*Il2ra*, *Cish*) and interferon response (*Ifitm1*, *Ifitm3*) (**Table S6**). Nevertheless, a fraction of T_{EX}^{prog}-(C1; Exhaustion-module "Conserved") and T_{MEM}-(C3; Memory module "Not Re-acquired)-related open chromatin regions were not or were more moderately affected by *ortho*IL-2 treatment suggesting selectivity in the epigenetic changes triggered by the *ortho*IL-2-Stat5 axis (**Fig. 7H**). Finally, the genomic regions remodeled in *ortho*IL-2 treated T_{EX}^{prog} ($T_{EX}^{[oIL2]}$), in particular the IL2-Stat5 C5 module also displayed consistent directionality of chromatin accessibility in P14 STAT5CA cells from d8p.i. (**Fig. S8C**). The susceptibility of those regions to IL-2/Stat5-mediated chromatin accessibility modulation at either early or late time-points of a chronic viral infections

554 suggested opportunities to leverage this IL-2/Stat5 axis for either the prevention or
555 therapeutic reprogramming of T_{EX} cells.
556
557 To examine the transcriptional circuitry that was rewired by *ortho*IL-2 signals in this setting
558 of T_{EX}^{prog} (re)differentiation, we next compared the network of TF binding site in the altered
559 chromatin accessibility landscape of T_{MEM}, $T_{EX}^{[PBS]}$ and $T_{EX}^{[oIL2]}$. The open chromatin
560 landscape of $T_{EX}^{[PBS]}$ enriched in binding motifs for TCR-inducible bZIP domain-containing
561 AP-1 family members ([C1]; i.e. Fra1/2, JunB, BATF, Atf3 or AP-1) and High Mobility
562 Group-TFs ([C2]; i.e. Tcf7, Tcf3, the Tcf7-homologue Lef1 and the Tcf7 partners Foxo1
563 and Eomes)[49-51] (**Fig. 7I**). T_{MEM}-derived cells, in contrast, enriched for T-box (i.e. Tbx21),
564 ETS (i.e. Ets1) and Runt (i.e. RUNX1/2) motifs (C3 and C4), consistent with distinct
565 transcriptional circuitry governing the T_{EX} and T_{MEM} lineages during recall
566 responses.[25,26,40,52] Notably, whereas T_{MEM} also contained accessible bZIP motifs, these
567 motifs were located in chromatin accessible regions associated with C4 DAP, whereas
568 the bZIP motifs enriched in $T_{EX}^{[PBS]}$ were found mainly in C1 open chromatin regions.
569 These data suggested distinct wiring of TCR-dependent signals (i.e. mediated via bZIP
570 TFs) in T_{EX} versus T_{MEM} during rechallenge. *Ortho*IL-2 treatment did not alter accessibility
571 at bZIP motifs in C1, the module associated with $T_{EX}^{[PBS]}$ recall responses. However,
572 *ortho*IL-2 increased accessibility at bZIP motifs in the T_{EFF}/T_{MEM}-related C4 and also
573 provoked increased accessibility at bZIP binding sites in C5, the module preferentially
574 enriched in the $T_{EX}^{[oIL2]}$ cells (i.e. Jun-AP1, Fosl2) (**Fig. 7I**). Thus, *ortho*IL-2, likely through
575 Stat5 engagement, appears to have a prominent impact in shaping the set of bZIP family
576 TF binding sites in T_{EX} during (re)differentiation. Moreover, *ortho*IL-2 treatment also

577 selectively reversed the T_{EX}-associated accessibility at HMG-TFs bound regions (C2) and
578 re-engaged T_{MEM}/T_{EFF}-related enhancers such as those bound by the Runx-family of TFs
579 (C4) (**Fig. 7I**). Together, these data suggest that providing strong (re)differentiation
580 signals via antigenic restimulation in combination with IL-2 and/or Stat5 signals may have
581 therapeutic potential to rewire T_{EX}. This augmented IL-2-Stat5-signaling during
582 (re)differentiation of T_{EX}^{prog} resulted in a remodeled epigenetic landscape and subsequent
583 reshaping of the TF network in these cells towards a hybrid T_{EFF}/T_{EX} state that combined
584 partial silencing and rewiring of exhaustion-related open chromatin regions to re-
585 engagement of some chromatin accessibility regions associated with the T_{EFF}/T_{MEM}
586 lineage.
587
588
589

Discussion

Reversing or rewiring the epigenetic program of T_{EX} remains a major goal of cancer immunotherapy.[11,13,25,53] Here, we discovered a reciprocal circuit between Stat5a and Tox in which Stat5a antagonizes Tox and the Tox-driven T_{EX} epigenetic program, fostering the acquisition of effector-like biology. In established T_{EX}, boosting Stat5 activity partially rewired the T_{EX} open chromatin landscape towards the T_{EFF}/T_{MEM} lineage with a preferential ability to function at the point of developmental flexibility that occurs as T_{EX}^{prog} convert to the "effector-like" T_{EX}^{int} subset. The use of an orthogonal IL-2/IL2Rβ-pair system[47] allowed Stat5-signals to be directed exclusively to the Ag-specific CD8 T cells of interest *in vivo* and strongly synergized with PD-1 pathway blockade through coordinated expansion of T_{EX}^{int} cells. These data may help explain the therapeutic benefit of IL-2 in settings of T cell exhaustion,[54,55] the combinatorial effect of IL-2 treatment with PD-1 pathway blockade,[48] and define mechanisms by which γ_c-cytokine signaling can impact CD8 T cell exhaustion. Moreover, a notable feature of manipulating Stat5 activity in T_{EX} was the generation of a highly durable hybrid state of differentiation that has features of effector biology, NK receptor expression, resistance to exhaustion, and durability which together, could have considerable therapeutic benefit.

IL-2 was one of the first effective immunotherapies for cancer[55] and, can have a direct impact on T_{EX}.[56] Our data now provide mechanistic explanations for these effects of IL-2. First, Stat5 antagonizes Tox and the Tox-dependent T_{EX} epigenetic imprinting fostering effector-like differentiation. This Stat5 antagonism of Tox may explain the preferential impact of early Stat5-signals in settings where Tox is abundant (chronic infections,

cancer) versus those that favor T_{EFF} (e.g. acutely resolving infections) where Tox expression is low.[7] Second, Stat5 was necessary for formation of T_{EX}^{int} cells a finding that may explain the strong synergy of IL-2 and PD-1 blockade. Mechanistically, Stat5 attenuated or extinguished the stem-like biology of T_{EX}^{prog} to initiate exit from quiescence, cell-cycle re-entry and allow downstream T_{EX}^{int} cell differentiation. One potential link between these events may be the mechanisms of downregulation of Tcf1 which is essential for exit from the T_{EX}^{prog} state.[27,35,57] In other settings, IL-2/Stat5-signals can repress Tcf1 activity and promote cellular differentiation.[58,59] Indeed, here we found that enhancing Stat5 activity (STAT5CA) depleted $Tcf1^{+}$ cells and provoked a loss of Tcf1 binding sites in established T_{EX} (*ortho*IL-2) whereas Stat5-deficiency trapped T_{EX} at the progenitor stage. Thus, the balance between Tcf1 and Stat5 activity may be one key regulator node for differentiation of T_{EX}^{prog} into downstream T_{EX} subsets including T_{EX}^{int}. Third, Stat5 promotes the effector circuitry in T_{EX}^{int} cells including driving expression of many effector (e.g. *GzmB*, *IFNγ*, *FasL or perforin*) and NK-related genes also previously linked to Stat5 activity in other settings.[38,58,60] Hence, Stat5 not only functions to drive formation of T_{EX}^{int} cells but also likely controls expression of some of the key genes associated with this effector/NK-like biology. Together, these observations provide rationale for developing therapeutic strategies to increase Stat5 activity in T_{EX} in settings of chronic infection or cancer. In particular, the *ortho*IL-2 approach[47] may control for previous limitations by delivering Stat5 inducing signals only to the cells of interest.[61]

Since the discovery of the distinct epigenetic wiring of T_{EX} that limits re-differentiation upon PD-1 blockade,[25,40] developing approaches to reprogram the epigenetics of T_{EX} has

been a major goal. Identifying such strategies, however, has proven challenging. The data presented here reveal new potential opportunities for, at least partial epigenetic re-wiring of T_{EX}. T_{EX} can retain epigenetic "scars" in settings of disease cure and rapidly re-engage the T_{EX} program upon antigenic rechallenge.[11,13,8,62] In settings of an acute viral rechallenge, we found that boosting the IL-2/Stat5 signals reversed a substantial fraction of these exhaustion-associated scars and restored accessibility at open chromatin regions associated with the T_{MEM}/T_{EFF} lineage. This partial epigenetic reprograming was sufficient to restore robust re-expansion and polyfunctionality. The exhaustion-specific open chromatin regions reversed by the IL-2/Stat5 axis were enriched for HMG-motifs especially those that could be bound by Tcf1. Tcf1 functions in activated CD8 T cells to maintain stemness at the expense of effector differentiation[49,50,57,63]. One possibility is that Tcf1 may restrain T_{EFF} features in T_{EX} and the ability of Stat5 signals to repress Tcf1 activity[58,59] maybe be sufficient to relieve the Tcf-mediated T_{EX}^{prog} restraint. Coupled to an antagonism of Tox, IL-2/Stat5 signals are likely to foster T_{EX} rewiring by both augmenting a developmental biology conversion of T_{EX}^{prog} into T_{EX}^{int} by antagonizing Tcf1 and also by removing the Tox-dependent reinforcement of the T_{EX} program. Thus, appropriately accessing the IL-2/Stat5 pathway provides a strong combination of signals for T_{EX} (re)differentiation.

Long-term persistence in settings of continued TCR signaling is a hallmark of T_{EX} cells compared to T_{EFF} or T_{MEM}.[14,15,35,64,65] Thus, a notable feature of constitutive Stat5a activity in Ag-specific CD8 T cells during chronic infection was the durability of this population despite the relative absence of the key regulators of T_{EX} persistence, Tox and Tcf1.[6-9,31-

[33,66] Although there are some data suggesting a role for IL-2-signals in fine-tuning memory CD8 T cell formation,[67] IL-2 signals also drive terminal differentiation of short-lived effector CD8 T cells and prolonged exposure to exogenous IL-2 exacerbates T_{EFF} contraction in settings of acute viral infection[54,68-72]. Moreover, use of IL-2 for *in vitro* expansion in settings of adoptive cell therapy (ACT) has been associated with poor engraftment and/or limited durability or anti-tumor activity of Ag-specific CD8 T cells.[59] Thus, although IL-2 fosters strong effector function, this cytokine can also drive terminal differentiation.[73,74] As a result, in settings of ACT, strategies to temper Stat5-signals (e.g. using engineered IL-2 variants or alternate γ_c-cytokines during *in vitro* expansion)[58,59,75] have been developed to restrain terminal differentiation and support formation of a stem-like compartment with superior engraftment potential and anti-tumor activity.[36,58,59,68,69,76,77] Thus, our data on the durability benefits of STAT5CA in chronic viral infection suggest several possibilities. First, constitutively active Stat5 may function differently than prolonged exposure to IL-2. Second, enforcing Stat5-signals directly in CD8 T cells may differ from exogenous IL-2 treatment, especially in settings where the ability of T_{EFF} signal downstream of IL-2 is reduced due to changes in receptor expression and/or signaling efficiency.[36,78,79] Third, continuous IL-2/Stat5 signals may provoke different effects than short-term IL-2 exposure as used in ACT protocols[59] or previous studies only providing additional IL-2 during the effector phase.[54] However, one last possibility is that in the setting of continuous TCR signals that drive exhaustion, enforced Stat5 activity synergizes with other exhaustion-driven antigen-dependent survival signals. Dissecting these questions will be an important future goal to determine how Stat5 interacts with other signals and devise strategies to optimally exploit the Stat5/IL-2 pathway for enhancing immunotherapy.

In summary, we identify a role for augmented IL-2/Stat5 signals in a potential epigenetic rewiring of T_{EX} cells and uncover the underlying molecular and cellular mechanisms for these effects. The result of increasing IL-2/Stat5 signals is a hybrid differentiation state combining therapeutically useful features of both T_{EFF} and T_{EX} leading to improved control of disease. The use of the *ortho*IL-2 system demonstrated that these effects are cell intrinsic to T_{EX} and suggests future strategies for Stat5 targeting therapeutics including cytokine-based and engineered cellular therapy-based approaches. Future studies in humans will be necessary to understand how these molecular principles extend to more complex settings with both pre-existing T_{EX} and opportunities for new T cell priming as well as role for other γ_c responsive cell types. Nevertheless, these data may provide a guide for developing and evaluating such therapies in future clinical trials.

STAR★METHODS

Mice

Six-week old C57BL/6 female mice (CD45.2, Charles River, NCI) were used as recipient mice for most adoptive transfer experiments. Alternatively, six-week old C57BL/6 male or female (CD45.2, The Jackson Laboratory) mice were used as recipients for Stat5iKO experiments. P14 TCR transgenic mice expressing a TCR specific for the LCMV D^bgp33-41 peptide were bred in house and backcrossed onto the C57BL/6 background. P14 $Rosa^{YFP}$ *Stat5a/b*$^{fl/fl}$ (P14 Stat5iKO) mice were generated by crossing *Stat5a/b*$^{fl/fl}$ mice (The Jackson laboratory, ref-#032053-JAX) with P14 $Rosa^{YFP}$ mice (bred in house). All experiments and breeding conditions were in accordance with Institutional Animal Care and Use Committee (IACUC) guidelines for the University of Pennsylvania.

Viruses and Infections

LCMV Arm and Cl13 were grown in BHK cells and titrated using plaque assay on VERO cells as described.[80] Recipient mice were infected either intraperitoneally (i.p.) with LCMV Arm ($2x10^5$ plaque forming units [PFU]) or intravenously (i.v.) with LCMV Cl13 ($4x10^6$ PFU).

Cell line and tumor transplant

The $B16_{gp33}$ melanoma cell line was maintained in DMEM supplemented with 10% FBS, 1% L-glut and 1% Pen/Strep. Tumor cells cultured for less than two weeks were resuspended in cold PBS and implanted subcutaneously ($5x10^5$ cells in 50μl) in the flank of recipient mice using 29G1/2 syringes. Tumor size was monitored every two days using

a digital caliper and mice were euthanized before tumors exceeded the volume permitted by the IACUC guidelines for the University of Pennsylvania.

Retroviral vectors

The STAT5CA construct has been described previously[36,37] and was kindly provided by Dr. Susan Kaech (The Salk Institute). The IL2Rβ-ortho construct has been described previously[47] and was obtained from Dr. Christopher K. Garcia (Stanford University) under the Material Transfer Agreement RIS#59882/00 between Stanford University, the University of Pennsylvania and the Parker Institute for Cancer Immunotherapy (PICI). Both constructs were cloned into a MSCV-IRES plasmid containing either VEX or YFP/GFP-reporters. RV particles were produced by transfection of 293T cells. Briefly, 293T cells were pre-incubated with warmed cDMEM supplemented with chloroquine (25μM; Sigma). Cells were transduced with a pCL-Eco plasmid (15μg) and MSCV-IRES expression plasmid (15μg) using Lipofectamine 3000 (ThermoFisher Scientific) for 6 hours at 37ºC 5%CO2. After incubation, transduction medium was replaced with fresh cDMEM. RV supernatants were collected at days 3 and 4 of culture and titrated on NIH3T3 cells.

METHOD DETAILS

Adoptive T cell transfer

PBMCs containing 1x10^3 P14 CD8 T cells were adoptively transferred into recipient mice 24h prior to infection with either LCMV Arm or LCMV Cl13. For Stat5iKO experiments, P14 Rosa$^{YFP+/-}$ *Stat5a/b*$^{fl/fl}$ (P14 Stat5iKO) and their control counterpart P14 Rosa$^{YFP+/-}$

741 *Stat5a/b*$^{+/+}$ (both CD45.1.2^{+}) were harvested from PBMCs and cultured in serum free
742 RPMI medium containing (cre+) or not (cre-) 50μg/ml of tat-cre recombinase (Proteomic
743 Core Facility-Children's Hospital of Philadelphia) for 45min at 37°C, 5%CO2. Cells were
744 washed once in FBS then complete RPMI (cRPMI), resuspended in cold PBS and 1.5x10^{3}
745 of each were adoptively transferred into separate naïve CD45.2 recipients 24h before
746 infection.[27] Markers associated with early T cell activation (i.e. CD69, Ly6C, PD-1, CD25,
747 CD62L, CD127) were assessed in P14 populations before infusion into recipient mice to
748 ensure transfer of phenotypically naïve T cells.
749
750 **Retroviral (RV) transduction**
751 RV transduction of P14 CD8 T cells was performed as described previously [81] with slight
752 modifications. For each experiment, P14 CD8 T cells were enriched from spleens of P14
753 transgenic mice using EasySep^{tm} CD8^{+} T cell isolation Kit (StemCell) and activated *in*
754 *vitro* in cRPMI supplemented with αCD3 (1μg/ml), αCD28 (0.5μg/ml) antibodies and rhIL-
755 2 (100U/ml) (PeproTech) at a seeding density of 1x10^{6} cells/ml. One day post activation
756 (between 24-27h), CD8 T cells were re-suspended at a density of 3-5x10^{6} cells/ml mixed
757 with RV supernatant containing polybrene (4μg/ml) at a 1:1 ratio (v/v) and spin-
758 transduced 75' at 2000g 32°C. After transduction, 4ml of warmed cRPMI containing
759 αCD3, αCD28 and rhIL2 was gently added to each well of a 6-well plate for a final volume
760 of 6ml. Cells were incubated O/N (~16h) at 37°C, 5% CO2. The next day, transduced
761 cells were stained for 15min with LiveDead Aqua (ThermoFisher Scientific) or Zombie
762 NIR (BioLegend) and anti-CD8 antibodies in 1XPBS at RT, resuspended in warmed
763 cRPMI and RV-positive cells (either VEX+ of YFP/GFP+) were sorted among live CD8 T

764 cells (LiveDead Aqua/Zombie NIR^{-}CD8^{+}). For most RV experiments described, P14 cells
765 expressing different congenic markers (CD45.1 or CD45.1.2) were used for transduction
766 of control RVs (empty) and RVs encoding proteins of interest (STAT5CA or IL2Rβ-ortho).
767 The two congenically distinct P14 populations were then mixed at a 1:1 ratio in warmed
768 PBS and injected into C57BL/6 recipients (2.5x10^{4} each) infected 3 days earlier with
769 LCMV Arm or Cl13.
770
771 **Tumor experiments**
772 C57BL/6 mice were inoculated with 5x10^{5} B16$_{gp33}$ cells. Ten days post tumor inoculation,
773 mice were randomized and either left untreated or injected i.v. with FACs purified P14
774 Empty or P14 STAT5CA cells (5x10^{5}).
775
776 **Cell preparation, flow cytometry and cell sorting**
777 Spleens were mechanically disrupted onto a 70μM cell strainer using the plunger of a
778 3mL syringe and resuspended in 1mL of ACK red blood cell lysing buffer (Gibco) for 3
779 min at room temperature (RT). Cell suspensions were washed and resuspended in
780 cRPMI supplemented with 10% FBS, 1% penn/strep, 1% L-glut, Hepes 10mM (Cell
781 Center, UPenn), MEM non-essential amino acids 1% (Gibco), Sodium Pyruvate 1mM
782 (Cell Center UPenn), β-mercaptoethanol (0.05mM). Bone marrow suspensions were
783 harvested by flushing cells out of the femur and tibia of infected mice with a 29G syringe
784 and cRPMI. Cells were then treated as above. For lungs and livers, mice were perfused
785 with cold PBS. Lungs were cut in a petri dish, disrupted in 10 ml of RPMI (1%FBS) in the
786 presence of Collagenase D (1X) (Roche) using a MACs dissociator (Miltenyi Biotec) and

incubated for 45min at 37°C under agitation. After incubation, lung cells were disrupted a second time on a MACs dissociator (Miltenyi Biotec) and processed as above. After mechanical disruption onto a 70μM strainer, lymphocytes from livers were enriched using Percoll (GE Healthcare) density gradient separation (80%/40%), washed two times with cRPMI and processed as above. Blood samples were collected in 1ml of PBS 2mM EDTA. RPMI was added (1ml) and samples were underlaid with 1ml of Histopaque 1083 (Sigma Aldrich) for lymphocyte enrichment using density gradient concentration. Remaining red blood cells were lysed using ACK lysing buffer (Gibco) for 3min at RT. Equal numbers of cell were stained with extracellular antibodies for 30min on ice in FACs buffer (PBS 1X, 1% FBS, 2mM EDTA) in the presence of Live/Dead Fixable Aqua Cell Stain (ThermoFisher Scientific). Cells were then fixed for 20 min on ice with Cytofix/Cytoperm (BD bioscience) and analyzed by flow cytometry. For cytoplasmic protein detection, cells were incubated for an additional 30min on ice in Perm/Wash buffer (BD bioscience) and stained for 1h on ice in Perm/Wash buffer (BD bioscience) containing antibodies targeting cytoplasmic proteins (active-caspase3, gzmA, gzmB, IFNγ, TNF). For TFs detection, cells were fixed (20min) and permeabilized (30min) on ice using the Foxp3 Transcription Factor buffer set (ThermoFisher Scientific) and incubated for an hour with TF antibodies. For TFs detection in cells expressing a fluorescent reporter protein (VEX or GFP/YFP), cells were pre-fixed 5min in 2% formaldehyde (ThermoFisher Scientific) before fixation and permeabilization using the Foxp3 TF buffer set (ThermoFisher

Scientific). Samples were resuspended in FACs buffer, acquired on an LSR II or BD FACSymphony and analysed with FlowJo v.10 software (Tree Star Inc).

For cell sorting *ex vivo*, CD8 T cells were enriched from total splenocytes using the EasySep^{tm} CD8^{+} T cell isolation Kit (StemCell) (routinely >90% purity), stained on ice for 30' with relevant cocktails of antibodies and populations of interest were sorted at 4^{o}C on an BD FACSARIA (BD Bioscience) using a 70 μM nozzle in 50% FBS RPMI. Purity was routinely >95%. For ATACseq, scRNAseq and CITEseq experiments, RV-positive or reporter expressing P14 cells (either VEX^{+} or GFP/YFP^{+}) were sorted among LiveDead Aqua/ZombieNIR^{-}CD8^{+}CD45.1^{+} cells. For re-challenge experiments, memory and T_{EX}^{prog} P14 cells were sorted among LiveDead Aqua^{-}CD45.1^{+}CD45.2^{-}CD8^{+} T cells and T_{EX}^{prog} cells were further discriminated as Ly108^{+}Cx3cr1^{-}.

Intracellular cytokine staining

Splenocytes or total CD8 T cells enriched using the EasySep^{tm} CD8^{+} T cell isolation Kit (StemCell) (1-2x10^{6}) were re-stimulated *in vitro* for 5h at 37^{o}C 5% CO2 in cRPMI supplemented with GolgiStop (1/250; BD bioscience), GolgiPlug (1/500; BD bioscience) and gp_{33-41} peptide (NIH, 0.4μg/ml). Cells were then washed and stained using the BD Fixation/permeabilization kit (BD Bioscience).

Antibody and cytokine treatment

Where indicated, mice were depleted of CD4 T cells using two i.p. injections of 200μL of PBS containing 200μg of monoclonal anti-CD4 antibody (clone GK1.5, BioXcell) one day prior and post infection with LCMV Cl13. PD-L1 blockade was performed in CD4-depleted mice as previously described.[25] Sequential i.p. injections of 200μl of PBS containing or not rat anti-mouse PD-L1 monoclonal antibody (200μg/injection, clone 10F.9G2, BioXcell) were performed every three days between days 22 and 34 for a total of five injections. For re-challenge experiments, similar injections were performed at d0, 3 and 6 post infection with LCMV Arm. For experiments using the IL2/IL2Rβ-orthogonal pair system, *ortho*IL-2 was infused daily (I.P) in 200μl of cold PBS at indicated concentrations from d21-to-25p.i. In some experiments, groups of mice were treated similarly with regular mIL2 as a reference (25KIU/injection). In experiments combining *ortho*IL-2 treatment with PD-L1 blockade, *ortho*IL-2 was infused I.P every 2 days (100KIU/injection) for the duration of PD-L1 treatment (d22-34p.i.). For re-challenge experiments, *ortho*IL-2 was infused daily (I.P) from d3-to-d7 post challenge (150KIU/injection).

Active caspase-3 and BrdU detection

Splenocytes from infected mice were incubated for 5 hours at 37°C 5%CO2 in cRPMI prior intra-cytoplasmic detection of active-caspase 3 (BD Bioscience) using BD Fixation/Permeabilization kit (BD Bioscience). Mice adoptively transferred with either P14WT or P14Stat5iKO were injected I.P with 2mg of BrdU at d7p.i. with LCMV Cl13 and

BrdU detection in splenic P14 cells was performed one day later (d8p.i.) using a BrdU detection Kit (BD Bioscience) according to manufacturer's protocol.

Sample preparation for Cut&Run

Cut&Run was performed as previously described [82] with modifications. P14 Empty and P14 STAT5CA cells were sorted at d8.p.i. with either LCMV Arm or Cl13 from recipients of two independent experiments and 0.5 to $3x10^5$ cells were recovered in 1.5ml DNA LoBind Eppendorfs containing 650µl of 50%FBS RPMI. Samples were washed twice in 1ml of cold wash buffer (20mM HEPES-NaOH pH7.5, 150mM NaCl, 0.5mM Spermidine and protease inhibitor from Roche), re-suspended in 400µl (final) of wash buffer containing 20µl of BioMagplus Concanavalin A-coated magnetic beads (Bangs Laboratories) per reaction and rotated for 15min at 4°C to allow the cells to bind. Tubes were placed on a magnet stand and liquid was removed. Beads were then incubated O/N at 4°C in 250µl of antibody buffer (20mM HEPES-NaOH pH7.5, 150mM NaCl, 0.5mM Spermidine, 2mM EDTA, 0.1% digitonin and protease inhibitor from Roche) containing 2.5µl (1/100) of antibodies against H3K27ac (Active Motif) or IgG control (Cell Signalling Tech). Samples were then washed twice in 500µl of Digitonin Buffer (20mM HEPES-NaOH pH7.5, 150mM NaCl, 0.5mM Spermidine, 0.1% digitonin and protease inhibitor from Roche), resuspended in 250µl of cold Digitonin Buffer containing Protein-A micrococcal nuclease (pA-MN) and rotated at 4°C for 1h. Beads were washed twice in 1ml of cold Digitonin Buffer to remove unbound pA-MN, resuspended in 150µl of Digitonin Buffer, cooled down at 0°C on a pre-cooled metal block for 5min and incubated 30min at 0°C with $CaCl_2$ (3µl of 0.1M per sample) to initiate pA-MN digestion. Reaction was

stopped by addition of 150µl of 2X stop Buffer (340mM NaCl, 20mM EDTA, 4mM EGTA, 0.02% Digitonin, 50µg/ml RNAseA and 50µg/ml Glycogen) followed by 10min incubation at 37°C to release target chromatin. Samples were then centrifuged 5min 16,000g 4°C and supernatants were transferred to new tubes. Chromatin fragments were incubated 10min at 70°C with 3µl of 10% SDS and 2.5µl of proteinase K (20mg/ml) followed by phenol/chloroform/isoamyl alcohol-based extraction according to original protocol (method B). Upper phase containing DNA was mixed with 1µl of glycogen (20mg/ml) and incubated with 750µl of cold 100% ethanol at -20°C O/N. Samples were centrifuged 30min 16,000g 4°C, rinsed once with 1ml of cold 100% ethanol and centrifuged again for 5min 16,000g 4°C to remove residual ethanol. Samples were air-dried, resuspended in 50µl of molecular grade water and stored at -20°C. DNA libraries were built using the NEBNext Ultra II DNA Library Prep Kit for Illumina (NewEngland Biolabs) with the following modifications.[83] NEBNext End Prep step was performed using 25µl of input material for a final volume of 30µl and the following adapted program (30min-20°C, 60min-50°C, Hold at 4°C). Adaptor was diluted at 1:25 and added at 1.5µl for ligation (15min-20°C) followed by addition of 1.5µl of Red USER Enzyme and additional 15min incubation at 37°C. Size selection was performed using 80µl of AMPure XP beads (Beckman Coulter) and purified DNA fragments were amplified for 14 cycles (annealing time changed to 10s). Libraries were cleaned-up with two rounds of size selection with AMPure XP beads (24µl/12µl; Beckman Coulter) and eluted in 15µl of molecular grade water, and amplicons quality was assessed on a 2200 TapeStation (Agilent Technologies). Libraries were quantified by qPCR using the NEBNext Library Quant kit for Illumina (NewEngland Biolabs) according to manufacturer's protocol and pooled at equal molarity (1nM). Denatured Libraries were

894 diluted at 1.8pM, loaded into a NextSeq 500/550 High Output Kit (75 cycles, Illumina) and
895 paired-end sequencing was performed on a NextSeq 550 (Illumina).
896
897 **Sample preparation for scRNAseq**
898 Splenocytes from recipient mice were pooled from duplicate experiments and CD8 T cell
899 enrichment was performed using EasySep^{tm} CD8+ T cell isolation Kit (StemCell).
900 Enriched CD8 T cells were stained and P14 populations of interest were sorted at 4^{o}C in
901 1.5ml Eppendorf tubes containing 50% FBS RPMI as described above. Sorted samples
902 were topped with cold PBS 0.04% BSA, centrifuged for 5' 350g at 4^{o}C, washed two times
903 in cold PBS and resuspended in 50-100μl of cold PBS. Samples were counted, down-
904 sampled and equivalent number of cells (6300) between samples were loaded into the
905 Chip (Chromium Next GEM Chip G) of a Chromium Next GEM Single Cell 3' Reagent Kit
906 v3.1 (Dual Index, 10x Genomics) and run onto a Chromium Controller. Samples were
907 then processed according to manufacturer's protocol. cDNA libraries were prepared using
908 the Dual Index TT Set A (10x Genomics) and the number of indexing PCR cycles was
909 adjusted to the cDNA input of each individual sample according to manufacturer's
910 recommendations. Libraries were quantified by qPCR using a KAPA Library Quant Kit
911 (KAPA Biosystems). Normalized libraries were pooled (2.5nM), loaded onto a NovaSeq
912 6000 SP Reagent Kit (100 cycles, Illumina) for a final concentration of 450pM and paired-
913 end sequencing was performed on a NovaSeq 6000 (Illumina).
914
915 **Sample preparation for CITEseq**

CITEseq samples from duplicate experiments were prepared as described above (scRNAseq section) and processed according to the CITE-seq protocol from the New York Center Technology Innovation Lab (https://cite-seq.com/protocols/). Briefly, enriched CD8 T cells were incubated for 10' at 4°C in Staining buffer (2%BSA/0.01% Tween in PBS) containing FcBlock (1/10 dilution ;TruStain™ FcX, Biolegend) followed by a 30' incubation in Staining Buffer containing TotalSeqB antibodies against Ly108, CD69, Tim-3, PD-1, CD127, CD122, Lag-3, CD38 and KLRG1 (BioLegend) previously titrated according to manufacturer's protocol using PE-conjugated version of each antibodies. Samples were then washed, sorted as described above, down-sampled and equivalent number of cells (10^4) between samples were loaded onto the Chip (Chromium Next GEM Chip G) of a Chromium Next GEM Single Cell 3' Reagent Kit v3.1 (Dual Index, 10x Genomics) and run onto a Chromium Controller. Samples were then processed according to manufacturer's protocol. Gene expression and Cell surface Protein libraries were constructed using Dual Index TT Set A and Dual Index NT Set A (10x Genomics) respectively. Libraries were quantified by qPCR using a KAPA Library Quant Kit (KAPA Biosystems). Normalized libraries were pooled (0.23nM), diluted to 1.8pg/ml and loaded onto a NextSeq 500/550 High Output Kit v2.5 (150 cycles, Illumina) and paired-end sequencing was performed on a NextSeq 550 (Illumina).

Sample preparation for ATACseq

ATACseq sample preparation was performed as described [41] with minor modifications. Sorted cells (2-to-5x10^4) were washed twice in cold PBS and resuspended in 50µl of cold lysis buffer (10mM Tris-HCl, pH 7.4, 10mM NaCl, 3mM MgCl2 and 0.1% IGEPAL CA-

630). Lysates were centrifuge (750xg, 10min, 4°C) and nuclei were resuspended in 50µl of transposition reaction mix (TD buffer [25µl], Tn5 Transposase [2.5µl], nuclease-free water [22.5µl]; (Illumina)) and incubated for 30min at 37°C. Transposed DNA fragments were purified using a Qiagen Reaction MiniElute Kit, barcoded with NEXTERA dual indexes (Illumina) and amplified by PCR for 11 cycles using NEBNext High Fidelity 2x PCR Master Mix (New England Biolabs). PCR products were purified using a PCR Purification Kit (Qiagen) and amplified fragments size was verified on a 2200 TapeStation (Agilent Technologies) using High Sensitivity D1000 ScreenTapes (Agilent Technologies). Libraries were quantified by qPCR using a KAPA Library Quant Kit (KAPA Biosystems). Normalized libraries were pooled, diluted to 1.8pM, loaded onto a NextSeq 500/550 High Output Kit v2.5 (150 cycles, Illumina) and paired-end sequencing was performed on a NextSeq 550 (Illumina).

QUANTIFICATION AND STATISTICAL ANALYSIS

FlowSOM analysis

Compensated parameters for gated P14 Empty and P14 STAT5CA cells were exported from four individual mice co-transferred with both P14 populations and concatenated. Concatenated files were down-sampled using the FlowJo DownSampleV3 plugin for even representation or P14 Empty and P14 STAT5CA populations (15000 cells each), grouped using the t-sne function of FlowJo V10.8.0 using 12 parameters (CD44, Tbet, Tcf1, Tim-3, GzmB, Tox, Lag3, Icos, Ly108, CD39, CD127 and PD-1) and clusters were defined with the FlowSom plugin using the same parameters.

Ingenuity Pathways Analysis (IPA)

DEGs between P14 WT and P14 ToxKO (**Fig. S1B**),[7] or cluster specific DEGs (**Fig. S1C-G**) from reprocessed scRNAseq of WT and ToxKO D^bgp33^+ CD8 T cells isolated at d7p.i. with LCMV Cl13 (GEO Accession number: GSE119943)[6] were used as input to the Upstream regulator analysis part of the Core analysis using QIAGEN's Ingenuity Pathway Analysis (IPA, QIAGEN Redwood City,www.qiagen.com/ingenuity) to generate Transcription factor specific networks.

Taiji Rank Analysis

Transcription Factor Binding Site (TFBS) analysis and PageRank analysis were performed using Taiji[34] (https://taiji-pipeline.github.io/algorithm_PageRank.html) and paired ATACseq and RNAseq datasets of indicated T_{EX} subsets (GEO accession number: GSE149879)[27] to generate TF ranks visualized as heatmap using R pheatmap package (**Fig. S1H**). For **Fig. 1A**, the fold change in Taiji score for T_{EX}^{int} cells compared to other T_{EX} subsets was calculated for each individual TF enriched in both the IPA analysis (**Fig. S1B**) and the Taiji Rank analysis (**Fig. S1H**).

ATACseq

Raw ATACseq FASTQ files from paired-end sequencing were processed using the script available at the following repository (https://github.com/wherrylab/jogiles_ATAC). Samples were aligned to the GRCm38/mm10 reference genome using Bowtie2. We used samtools to remove unmapped, unpaired, mitochondrial reads and ENCODE blacklist regions were also removed

(https://sites.google.com/site/anshulkundaje/projects/blacklists). PCR duplicates were removed using Picard. Peak calling was performed using MACS v2 (FDR q-value 0.01). For each experiment, we combined peaks of all samples to create a union peak list and merged overlapping peaks with BedTools *merge*. The number of reads in each peak was determined using BedTools *coverage.* Differentially accessible peaks were identified following DESeq2 normalization using a lfc of 2 and FDR cut-off <0.01 unless otherwise indicated. DAPs were clustered using the k-means clustering methods and motif enrichment analysis was performed for each cluster on indicated DAPs using Homer (default parameters). For peak tracks representation, bed files for each replicate were imported into the UCSC Genome browser online tool. Replicates for each sample were merged and each biological sample were normalized. For sample distance, a distance matrix was calculated using the “euclidean” measure for all peak and plotted as a heatmap.

CUT&RUN and ChIP-Seq data processing and analysis

Data qualities were checked using FastQC and MultiQC. Paired-end reads were aligned to mm10 reference genome using Bowtie2 v2.3.5 with options suggested by Skene et *al*. 2018.[82] Bam files containing uniquely mapped reads were kept using Samtools v1.1. MarkDuplicates command from Picard tools v1.96 was used to remove presumed PCR duplicates. Blacklist regions defined by ENCODE were removed, and filtered typical chromosomes were used for downstream analysis. Read per million (RPM) normalized bigwig files to visualize binding signals were created using deepTools bamCoverage v3.3.2 with parameters --normalizeUsing CPM -bs 5 –smoothLength 20 –skipNAs.

Biological replicates were pooled together using bigwigCompare with parameter --operation add -bs 5 --skipNAs. Peaks were called on using MACS v2.1 using the broadPeak setting with general adjusted *p*-value cutoff of 0.05. Genes proximal to peaks were annotated against the mm10 genome using R package rGREAT. Venn diagram of peak comparisons were plotted using Bioconductor package ChIPpeakAnno. Peaks of all conditions were merged to create the final union peaks list. For visualization purpose, bigwig files of biological replicates were pooled using wiggletools with mean setting, and median background were subtracted. Tracks were loaded to UCSC genome browser for visualization. Published ChIP-Seq data were downloaded from NCBI (GEO accession number: GSE64407 [Nfat1], GSE98654 [Nfat2], GSE100674 [Stat5]).[42,43,84] Paired-end reads were aligned to mm10 reference genome using Bowtie2 with same parameters as CUT&RUN. RPM normalized tracks were generated using deepTools bamCoverage. Some downloaded signal track files were lifted from mm9 to mm10 using UCSC tool liftOver. Read counts under peaks were generated using deepTools multiBigwigSummary v3.3.2. Binding motifs enrichment analysis were identified using findMotifsGenome.pl from HOMER v4. Local motif binding positions are identified using FIMO with parameters –bfile –motifs. Dot plots were generated using R packages ggplot2.

Single-Cell RNA sequencing (scRNAseq)

Sample demultiplexing, alignment, filtering and creation of a UMI count matrix were performed using Cell Ranger software v.4.0.0 (10x Genomics). A Seurat object was created from the UMI count matrix using Seurat_4.0.5.[85] Cells with fewer than 200 or greater than 2500 detected genes were excluded from downstream analysis as of cells

with >10% of mitochondrial gene counts. Genes which expression was detected in 3 cells or less were excluded. A total of 920 P14 Empty and 302 P14 STAT5CA cells passed filters with an average sequencing depth of 1984 genes per cell and were considered for downstream analysis. Counts were normalized by total expression in the corresponding cell using the "LogNormalize" function and default scaling factor of 10,000 to give counts per million. Top 2000 variable features were determined using the "vst" selection method. Linear dimensional reduction (PCA) was performed on scaled variable features and features from the 20 most significant PCs were used as input for unsupervised clustering using the "FindNeighbors" and "FindClusters" functions of Seurat with a resolution of 0.3. We next ran non-linear dimensional reduction (UMAP) to visualize the data. Differentially expressed genes were identified by the Seurat function "FindAllMarkers" with min.pct=0.25 and logfc.threshold=0.25 and the top 10 genes per cluster were used for creating the Heatmap using the R package "Dittoseq" (**Fig. S4F**). For projection of indicated gene signatures (SLEC, Exhaustion, Tox program and T_{EX}^{prog1}, T_{EX}^{prog2}, T_{EX}^{int}, T_{EX}^{term}), Seurat clusters were used as features to calculate module scores of single cells using the "AddModuleScore" of Seurat_4.0.5. Module scores for each of the gene signatures were used to color the UMAP projection (**Fig. S4G**) or dot plots (**Fig. 4F**). Single-cell analysis of P14 Empty and P14 IL2Rβ-ortho was processed independently using similar pipeline. A total of 925 P14 Empty and 951 P14 IL2Rβ-ortho passed filters with an average sequencing depth of 1786 genes per cell and were considered for downstream analysis. Non-linear dimensional reduction (UMAP) was used to visualize data (**Fig. S7E,F**) from the 12 most significant PCs using a resolution of 0.1.

For projection of Stat5a and Tox signatures, scRNAseq data of P14 CD8 T cells isolated from LCMV Cl13 infected mice at d7 and d30p.i. (GEO accession number: GSE131535 and GSE150370),[11,35] were reprocessed and module scores for Stat5a and Tox signature genes were used to color the UMAP (**Fig. 1B**) as described above.

Cellular Indexing of Transcriptomes and Epitopes by sequencing (CITE-seq)

A UMI count matrix was created for P14 WT and P14 Stat5iKO cells using CellRanger 4.0.0. and the two matrixes were used to create Seurat objects. For each sample, an antibody ("adt") assay was created and added to its cognate Seurat object (WT or Stat5iKO) that were subsequently merged into one object containing rna and adt counts for each sample. Cells with fewer than 200 or greater than 2500 detected genes were excluded from downstream analysis as of cells with >12% of mitochondrial gene counts. Genes which expression was detected in 3 cells or less were excluded. A total of 4377 P14 WT and 4906 P14 Stat5iKO cells passed filters with an average sequencing depth of 1210 genes per cell and were considered for downstream analysis. Counts (rna assay) were then normalized, and the top 2000 variable features were scaled before running linear dimensional reduction (PCA). The 30 most significant PCs were used as input for unsupervised clustering using the "FindNeighbors" and "FindClusters" functions of Seurat with a resolution of 0.1. We next ran non-linear dimensional reduction (UMAP) using the rna assay to visualize Seurat clusters (**Fig. 5F**) or individual samples (**Fig. 5G**). DEGs were identified by the Seurat function "FindAllMarkers" with min.pct=0.25 and logfc.threshold=0.25 and the top 52 variable features by p.val.adj were used for creating the Heatmap (Fig. 5H). The "FindMarkers" function of Seurat was also used for cluster-

wise assessment of the number of DEGs using as an input Seurat clusters (**Fig. S6C**) or oligo-tagged antibodies-defined populations (**Fig. 5I**). These oligo-tagged defined populations were delineated based on Ly108 and CD69 adt values with cut-off for positive and negative cells set up using the "FeatureScatter" function of Seurat. DEGs between oligo-tagged defined populations were presented as Volcano plots (**Fig. 5J**). For projection of indicated gene signatures (T_{EX}^{prog1}, T_{EX}^{prog2}, T_{EX}^{int}, T_{EX}^{term}), oligo-tagged defined populations were used as features to calculate module scores of single cells using the "AddModuleScore" of Seurat_4.0.5. Module scores for each of the gene signatures were used to color the UMAP projection (**Fig. S6E**) or dot plots (**Fig. S6F**).

Gene ontology

Gene ontology of gene sets of interest were obtained using the Metascape online tool (http://metascape.org/gp/index.html#/main/step1). Pathway enrichment analysis (GO Biological processes) was set for a minimum overlap of 3, a *p*-value cut-off of 0.01 and a minimum enrichment score of 1.5.

Statistical analysis and experimental replications

Statistics on flow cytometry data were performed using unpaired or paired (co-adoptive transfer experiments) two-tailed Student's t test. For data presented as a ratio (**Fig. 2D-E, 4B, 5A, and 6F,I**) a Wilcoxon signed rank test was performed with a hypothetical value of 1 or equal to the mean in control group (**Fig. 6F,I**) (GraphPad Prism v6; *p < 0.0332, **p < 0.0021, ***p < 0.0002, ****p < 0.0001). For statistics on scRNAseq data, a Pearson correlation coefficient was calculated as well as a *p* value of significance to estimate the

degree of correlation between Stat5a and Tox signatures (**Fig. 1C** and **S1I**). A Wilcoxon t test was performed in **Fig. 4I** to compare enrichment of indicated signature in T_{EX} clusters.

The experiments described were replicated as follows. **Figure 2** - (**B**) N=3 independent experiments (ind exp) with 12 mice/group (**D**) N=2 (Tcf1) or 4 (Tox) with 8 (Tcf1) or 15 (Tox) mice/group (**E**) N=2-4 ind exp with 6-16 mice/group (**F-G**) N=3 ind exp with 10-12 mice/group (**H**) N=2 with 7-9 mice/group. **Figure 4** - (**A**) Representative of 2 ind exp with 10 mice/group (**B**) N=2-4 ind exp with 5-17 mice per time points (**C**) Representative of 2 ind exp with 9-10 mice/group (**K-L**) Representative of 2 ind exp with at least 6 mice/group in each. **Figure 5** - (**A**) N=2-5 ind exp with 6-18 mice/group (**B**) N=4 ind exp with 14 mice per group (**C**) N=3 ind exp with 9-10 mice/group (**D**) N=1-2 ind exp with 2-8 mice/group (**E**) Representative of 2 ind exp with 8-10 mice per group. **Figure 6** – (**B**) N=2 ind exp with 6-10mice/group (**C**) N=2 with 6 mice/group (**D**) N=2 with 6-17 mice/group (**F-I**) N=2 with 9-15 mice per group. **Figure 7** - (**B**) N=5 with 5-18 mice/group (**C**) N=2 with 2-8 mice/group (**D**) Representative of 5 in exp with 5-18 mice/group (**E**) N=5 with 5-18 mice/group.

Acknowledgments

We thank all members of the Wherry Lab and Dr. Golnaz Vahedi (UPENN) for insightful discussions and comments on the manuscript as well as Dr. Susan Kaech (Salk Institute for Biological Studies) for providing the original STAT5CA constructs. This work was supported by the Parker Institute for Cancer Immunotherapy (PICI) and the National Institute of Health (NIH) grants AI155577, AI115712, AI117950, AI108545, AI082630 and

CA210944 (to EJW). ACH is supported by NIH (K08CA230157) and received Doris Duke Clinical Scientist Development and Damon Runyon Clinical investigator Awards. JC-B is a Parker Institute for Cancer Immunotherapy (PICI) scholar. DM was supported through The American Association of Immunologists Intersect Fellowship Program for Computational Scientists and Immunologists.

Author Contributions

JC-B and EJW conceived and designed the experiments. JC-B performed the experiments with help from MSA-H, YM, VC, DM, JB and MK. JC-B prepared libraries and performed sequencing with help from DM and ACH. JC-B analyzed the scRNAseq and CITE-seq datasets with help and guidance from SM. ATACseq datasets were analyzed by SM and HH in collaboration with JC-B. ZZ and SL-B provided technical help for CnR and CnR datasets were analyzed by HH in collaboration with JC-B. LS, LP and K-CG provided the orthogonal IL2Rβ construct. MK adapted the STAT5CA construct to our MSCV based expression system. JC-B and EJW wrote the manuscript with input from MSA-H, JRG, HD and ACH.

Conflicts of Interest

ACH is a consultant for Immunai and receives research support from BMS. K-CG is the founder of Synthekine. EJW is a member of the Parker Institute for Cancer Immunotherapy which supported the study. EJW is an advisor for Arsenal Biosciences, Merck, Marengo, Janssen, Related Sciences, Pluto Immunotherapeutics, Rubius,

Synthekine, and Surface Oncology. EJW is a founder of Surface Oncology, Danger Bio, and Arsenal Biosciences.

Data availability

All sequencing data generated during this study will be made publicly available at the time of publication.

Figure legend

Figure 1: Reciprocal Activity between Stat5a and Tox in Ag-specific CD8 T cells during chronic infection. **A**- Dot plot of IPA regulators significantly enriched from **Fig. S1B** (logp≥10) that were also enriched in an independent Taiji Rank analysis in **Fig. S1H**. Selected IPA regulators are plotted based on their fold change in Taiji enrichment for T_{EX}^{int} cells (Y axis) and correlation of the IPA-defined gene network for each TF to Tox expression (X- axis). **B**- UMAP of re-processed scRNAseq of P14 CD8 T cells at d8 (upper panel)[35] or d30 (lower panel)[11] post Cl13 infection projecting the Stat5a network as defined by the IPA analysis (left) or a core signature for Tox (genes enriched in P14 WT versus P14 ToxKO).[7] **C**- Correlation scores between Stat5a network and a Tox signature at indicated time of Cl13 infection.

Figure 2: Stat5 opposes Tox and antagonizes establishment of exhaustion. A- Experimental design. **B**- Frequency of Ly108/Tim-3-defined subsets in indicated populations at d8p.i. **C**- t-sne representation of flow cytometry data highlighting FlowSOM clusters (see methods). **D**- Tcf1 and Tox expression in indicated populations at d8p.i. **E**- MFI of indicated markers expressed as a ratio (P14 STAT5CA/P14 Empty). **F**- Frequency of Ly108/Tim-3-defined subsets in indicated populations at d8p.i. **G**- Absolute numbers of indicated populations at d8p.i. **H**- Tox expression in indicated sub-populations of P14 WT and P14 Stat5iKO at d8p.i.

Figure 3: Enhanced Stat5a activity restrains Tox and the Tox-dependent exhaustion program while supporting an effector epigenetic landscape. Splenic P14 Empty and

P14 STAT5CA cells isolated at d8 of Cl13 infection were analyzed by ATACseq. Naïve CD8 T cells (not depicted) and P14 cells isolated from Arm infected mice at d8p.i. (T_{EFF}) were used as reference. **A**- PCA of normalized ATACseq counts (all peaks). **B**- Number of peaks more accessible in indicated populations and comparisons (FDR 0.01, lfc≥2). **C**- Clustered heatmap (k-means) of DAPs between P14 Empty and P14 STAT5CA (FDR 0.01, lfc≥2) annotated with most variable genes per cluster (among top 100 per cluster by lfc and number of DAPs). **D**- Top 10 motifs (Homer) enriched in DAPs from corresponding clusters in **Fig.3C**. **E**- Heatmap for scores associated with genomic regions plotting accessibility at genes from indicated gene signatures list. **F**- Frequency of genes from signature list in **Fig. 3E** with DAPs between P14 Empty and P14 STAT5CA that possess direct binding sites for Stat5 (chipseq dataset from *Villarino et. al, J Exp Med 2017*).[84] **G**- Dot plot of exhaustion signature genes (**from Fig. 3E**-middle) containing at least 3 DAPs between P14 Empty and P14 STAT5CA cells and scored based on the number of DAPs per gene (Y axis), average lfc (X axis) and number of direct Stat5 binding sites (bubble size). **H**- ATACseq, Cut&Run (H3K27ac) and Chip-seq (NFAT1,[42] NFAT2[43] and Stat5[84]) tracks at the Tox locus. Blue highlights indicate ATAC peaks reduced in P14 STAT5CA cells compared to P14 Empty. **I**- ATACseq track zoom-in from **Fig. 3H**. **J**- Top 10 motifs (Homer) enriched in DAPs between P14 Empty and P14 STAT5CA found at the Tox locus.

Figure 4: Constitutive Stat5a activity drives a durable and protective effector/NK-like CD8 T cell differentiation during chronic viral infection and cancer. A- Frequency of co-transferred P14 Empty and P14 STAT5CA cells among RV+ (VEX+)

CD8 T cells at d27p.i. with Cl13 (left) or Cl13 with CD4-depletion (right). **B**- Ratio of cell number (P14 STAT5CA/P14 Empty) at indicated time points in the spleen. **C**- Frequency of Ly108/CD69-defined T_{EX} subsets in indicated populations at d27p.i. **D**-**E** UMAP of scRNAseq data combining P14 Empty^{VEX+} and P14 STAT5CA^{VEX+} cells isolated at d27p.i. plotting Seurat clusters (**D**-left) or individual samples (**E**) and representative genes per cluster (**D**-right). **F**- GSEA for indicated signatures in Seurat clusters. **G**- DEGs (log2FC>0.5, p_value_adj≤0.05) between C2 and C3 from **Fig. 4D**. **H**- Gene ontology for genes Up in C2 vs C3 from (**Fig. 4D**) **I**- Relative expression of genes with increased accessibility in P14 STAT5CA over P14 Empty at d8p.i. (**Fig. 3**) across Seurat clusters. **J**- Experimental design. **K-L**- $B16_{gp33}$ tumor growth (**K**) and Kaplan Meyer survival curve (**L**) for each experimental group.

Figure 5: Stat5-signals drive T_{EX}^{int} cell development and are essential for CD8 T cell responses to PD-L1 blockade. A- Expression of key markers on indicated splenic populations at d27p.i. **B**- Frequency of Ly108/CD69-defined subsets among indicated populations at d27p.i. **C-** Absolute numbers of indicated populations of P14 WT and P14 Stat5iKO cells at d27p.i. **D**- Absolute numbers of T_{MEM} and Ly108^{+} T_{EX}^{prog} in indicated P14 populations at d27 post Arm (Arm, memory) or Cl13 (Cl13, Ly108^{+} progenitors) infection with (YFP^{+}cre^{+}) or without (YFP^{-}cre^{-}) prior *in vitro* treatment with tat-cre recombinase. **E**- Frequency of Ly108/CD69-defined subsets among P14 WT and P14 Stat5iKO cells at d35p.i. in CD4 T cells-depleted hosts treated (αPD-L1) or not (PBS) with anti-PD-L1 antibodies between d22-34 (see method). **F**-**G**- UMAP plotting RNA-defined Seurat clusters (**F**-left) or individual samples (**G**) from CITE-seq analysis of P14 WT and P14

Stat5iKO cells isolated at d27p.i. **H**- Top 52 DEGs between P14 WT and P14 Stat5iKO. **I**- Number of DEGs between oligo-tagged antibodies (Ly108 and CD69)-defined populations (see **Fig. S6D,E**). **J**- DEGs (FC≥0.25) between indicated oligo-tagged antibodies (Ly108 and CD69)-defined populations of P14WT and P14 Stat5iKO cells.

Figure 6: Orthogonal IL-2/IL2Rβ-triggered Stat5 activation in Ag-specific CD8 T cells enforces T_{EX}^{int} cell development and synergizes with PD-L1 blockade. A- Experimental design. **B**- Absolute numbers of YFP^+ P14 Empty and P14 IL2Rβ-ortho cells isolated at d26p.i. from experimental groups infused with indicated concentration of *ortho*IL-2. **C-** Frequency of Ly108/CD69-defined subsets among co-transferred P14 $Empty^{YFP+}$ and P14 IL2Rβ-$ortho^{YFP+}$ cells isolated at d26p.i. from indicated experimental groups. **D**- Frequency of indicated subsets among P14 IL2Rβ-$ortho^{YFP+}$ cells isolated at d26p.i. from experimental groups infused with indicated concentrations of *ortho*IL-2. Dotted grey lines indicate mean frequencies of each sub-population across all experimental groups in P14 IL2Rβ-$ortho^{YFP-}$ control cells. **E**- Experimental design. **F**- Ratio of cell number between co-transferred P14 IL2Rβ-$ortho^{YFP+}$/P14 $Empty^{YFP+}$ in indicated experimental groups at d35p.i. Combo stands for αPD-L1+*ortho*IL-2 (100KIU). **G**- Relative frequency of P14 $Empty^{YFP+}$ and P14 IL2Rβ-$ortho^{YFP+}$ cells in indicated experimental groups at d35p.i. **H**- Representative dot plots of Ly108/CD69-defined subsets among P14 $Empty^{YFP+}$ and P14 IL2Rβ-$ortho^{YFP+}$ cells isolated at d35p.i. from indicated experimental groups. **I**- Ratio of absolute cell number between indicated subsets of co-transferred P14 IL2Rβ-$ortho^{YFP+}$ and P14 $Empty^{YFP+}$ isolated at d35p.i. from indicated experimental groups.

Figure 7: Improved function and partial epigenetic rewiring of rechallenged T_{EX}^{prog} cells with targeted IL-2-Stat5 signals. A- Experimental design. P14 Memory (Memory) and P14 Ly108^{+} T_{EX} progenitors (YFP^{+}, expressing the IL2Rβ-ortho receptor, [T_{EX}]) were sorted from indicated time post Arm (d≥90p.i.) or Cl13 (d26p.i.) infection respectively (see **Fig. S8A** for sorting strategy), transferred into new hosts and challenged with LCMV Arm. Mice injected with T_{EX} cells (Ly108^{+} P14 expressing IL2Rβ-ortho^{YFP+}) were treated with either PBS ($T_{EX}^{[PBS]}$) or daily infusion of *ortho*IL-2 (150KIU day 3-7; [$T_{EX}^{[oIL2]}$) in combination or not with αPD-L1 blockade (day0, -3 and -6p.ch.). P14 memory cells were treated with PBS or αPD-L1 at similar time points. Cells were analyzed in the spleen at d8p.ch. **B**- Absolute numbers in the spleen at d8.p.ch. **C**- Cytokine secretion by re-challenged memory and T_{EX} from each experimental conditions after 5h of *in vitro* re-stimulation with gp33 peptide. **D**- Expression of indicated markers on re-challenged memory and T_{EX} from each experimental condition. **E**- Frequency of KLRG1/CD127-defined sub-populations among re-challenged memory and T_{EX} from indicated experimental groups. **F**- PCA of ATACseq data using all DAPs (FDR 0.01, lfc≥2) between indicated populations isolated at d8p.ch. **G**- Number of peaks more accessible in indicated populations and comparisons (FDR 0.01, lfc≥2). **H**- Clustered heatmap (k-means) plotting all DAPs between indicated populations (FDR 0.01, lfc≥2). **I**- Motif enrichment analysis (Homer) plotting the top 10 motifs enriched in DAPs from corresponding clusters in **Fig.7H**.

Supplemental figure legend

Figure S1 (related to Figure 1): Increased Stat5a activity in T_{EX}^{int} and ToxKO CD8 T cells. **A**- Analytical approach. **B**- Ingenuity Pathways Analysis on DEGs between P14 WT and P14 ToxKO cells at d8p.i. (dataset from *Khan et. al, Nature 2019*).[7] Transcriptional regulators significantly enriched (logp>10) in P14 WT or P14 ToxKO are highlighted in grey and blue respectively. Non-significant hits are colored in black. Bubble size represents the number of genes considered by the IPA analysis for each individual TF. **C**- UMAP of re-processed scRNAseq data of WT and $Tox^{-/-}$ gp_{33}-specific CD8 T cells isolated from bone marrow chimeras at d7 post LCMV Cl13 infection and featuring Seurat clusters.[6] **D**- Histogram showing the relative proportion of WT and $Tox^{-/-}$ CD8 T cells in each Seurat cluster from **Fig. S1C**. **E**- Heatmap of top10 DEGs between WT and $Tox^{-/-}$ $gp33^{+}$ CD8 T cells per indicated cluster identified in **Fig. S1C**. **F**- IPA analysis of DEGs between WT and $Tox^{-/-}$ $gp33^{+}$ CD8 T cells for each individual cluster defined in **Fig. S1C**. Plotted are the top 10 transcriptional regulators enriched in each individual cluster. **G**- Network analysis of Stat5a and T-bet (*Tbx21*) by Ingenuity of DEGs between WT and $Tox^{-/-}$ $gp33^{+}$ CD8 T cells in indicated clusters form **Fig. S1C.** Darker red in target genes indicates positive enrichment in $Tox^{-/-}$ $gp33^{+}$ CD8 T cells. **H**- Taiji rank analysis identifying TFs with increased activity in previously defined subsets of T_{EX} based on published RNAseq and ATACseq data.[27] Plotted are overlapping TFs identified in both the IPA analysis in **Fig. S1B** and the independent Taiji analysis. **I**- Correlation scores between Stat5a network and indicated gene signatures at d30 post LCMV Cl13 infection.

Figure S2 (related to Figure 2): Stat5 impacts early cell-fate decision of Ag-specific CD8 T cells during a chronic viral infection. A- MFI of indicated markers expressed as a mean of ratio (P14 Ly108^{+}Tim-3^{-}/P14 Ly108^{-}Tim-3^{+}). N=10 with 4-20 mice/group. **B**- Numerical proportion of P14 Empty (grey) and P14 STAT5CA (blue) within indicated populations of VEX^{+} cells at d8p.i. N=4 with 16 mice/group. **C**- Representative dot plot (left) and cumulative frequencies (right) of IFNγ and TNFα production by P14 Empty (grey) and P14 STAT5CA (blue) cells at d8p.i. N=2 with 8 mice/group. **D**- Experimental design. PBMCs from CD45.1.2^{+} P14 Rosa^{YFP}*Stat5a/b*$^{+/+}$ (P14 WT) and P14 Rosa^{YFP}*Stat5a/b*$^{fl/fl}$ (P14 Stat5iKO) mice were treated (cre+) or not (cre-) with Tat cre recombinase *in vitro* and adoptively transferred into separate groups of C57BL/6J recipients subsequently infected with LCMV Cl13. Transferred cells were tracked at d8p.i. using congenic markers and YFP induction was used as a surrogate of cre-mediated recombination and deletion of floxed alleles. **E**- Representative contour plots (left) and cumulative frequencies (right) of Ly108 and Tim-3-defined subpopulations among untreated (cre-, YFP^{-}) P14 WT (grey) and P14 Stat5iKO (blue) control cells at d8p.i. Numbers indicate frequencies. N=3 with 11-12 mice/group. **F**- Absolute numbers of indicated populations among untreated (cre-, YFP^{-}) P14 WT (grey) and P14 Stat5iKO (blue) control cells at d8p.i. N=2 with 6-7 mice/group. **G**- *In vivo* BrdU incorporation (d7 to d8p.i.) in indicated populations of untreated (cre-, YFP^{-}) and treated (cre+, YFP^{+}) P14 WT (grey) and P14 Stat5iKO (blue) cells at d8p.i. **H**- Active caspase 3 staining in indicated populations of untreated (cre-, YFP^{-}) and treated (cre+, YFP^{+}) P14 WT (grey) and P14 Stat5iKO (blue) cells at d8p.i, after 5h incubation at 37^{o}C. **I**- Representative dot plots of KLRG1 and CD127-defined subpopulations among treated (cre+, YFP^{+}) and untreated (cre-, YFP^{-}) P14 WT (grey)

and P14 Stat5iKO (blue) cells isolated from the blood at d8 post LCMV Arm infection. Numbers indicate frequencies. (G-I) N=2 with 3-8 mice/group.

Figure S3 (related to Figure 3): Constitutive Stat5a activity drives a hybrid epigenetic state in Ag-specific CD8 T cells. **A**- Spearman distance analysis using all DAPs (FDR≤0.01, lfc≥2) between indicated populations. Color indicates distances. **B**- Genetic distribution of the total peak list (upper panel) and all DAPs between T_{EFF}, P14 Empty and P14 STAT5CA cells (lower panel; FDR≤0.01, lfc≥2). **C**- Overlap between genes containing DAPs between P14 Empty and P14 STAT5CA and genes differentially expressed between WT and *Tcf7*$^{-/-}$ P14 cells (dataset from *Wu et. al*[33]) **D**- ATACseq tracks of indicated genes. DAPs between P14 Empty and P14 STAT5CA are highlighted in blue. **E**- Clustered heatmap (k-means) plotting all DAPs between P14 Empty, P14 STAT5CA and T_{EFF} cells (FDR≤ 0.01, lfc≥2).

Figure S4 (related to Figure 4): Constitutive Stat5a activity increases durability and effector biology in CD8 T cells during chronic viral infection. A- Pre-adoptive transfer mix plotting the relative frequency of P14 Empty^{VEX+} over P14 STAT5CA^{VEX+} prior to adoptive transfer. **B**- Relative frequencies of P14 Empty (grey) and P14 STAT5CA (blue) among VEX^{+} CD8 T cells at d27p.i. N=2 with 10 mice/group. **C**- Number of P14 Empty^{VEX+} (grey) and P14 STAT5CA^{VEX+} (blue) per 10^6 CD8 T cells in indicated anatomical locations. Data representative of 2 independent experiments with 5 mice/group in each. **D**- Representative dot plot (left) and cumulative frequencies (right) of P14 Empty (grey) and P14 STAT5CA (blue) isolated from the spleen of LCMV Cl13 and CD4-depleted mice at

d≥90p.i. Numbers indicate frequencies. N=2 with 6 mice/group. **E**- Frequencies of indicated populations among P14 Empty^{VEX+} (grey) and P14 STAT5CA^{VEX+} (blue) cells at d27p.i. N=2 with 9-10 mice/group. **F**- Heatmap displaying the top 10 variable genes per Seurat clusters (defined in **Fig. 4D**) at d27p.i. **G**- Projection of indicated T_{EX} subset signatures (dataset from *Beltra et. al* [27]) into UMAP space from **Fig. 4D**. **H**- Relative distribution of indicated P14 populations across Seurat clusters (defined in **Fig. 4D**).

Figure S5 (related to Figure 5): Stat5 is essential to maintain CD8 T cell responsiveness to PD-L1 blockade in settings of chronic viral infection. A- Representative contour plots (left) and cumulative frequencies (right) of Ly108 and CD69-defined subpopulations among untreated (cre-, YFP$^-$) P14 WT (grey) and P14 Stat5iKO (blue) control cells at d27p.i. Numbers indicate frequencies. N=4 with 10-12 mice/group. **B**- Absolute numbers of indicated populations among untreated (cre-, YFP$^-$) P14 WT (grey) and P14 Stat5iKO (blue) control cells at d27p.i. N=3 with 5-8 mice/group. **C**- Number of treated (cre+, YFP$^+$) P14 WT (grey) and P14 Stat5iKO (blue) cells per 10^6 CD8 T cells in indicated anatomical location at d27p.i. Numbers indicate fold changes in cell numbers. **D**- Representative dot plots displaying the frequency of treated (cre+, YFP$^+$) P14 WT (grey) and P14 Stat5iKO (blue) cells among gp33$^+$ CD8 T cells in indicated anatomical locations at d27p.i. (C-D) N=1 with 3 mice/group. **E**- Cumulative frequencies of Ki67$^+$ cells among indicated populations of P14 WT and P14 Stat5iKO cells at d27p.i. N=3 with 10-11 mice/group. **F**- Absolute numbers of P14 WT (grey) and P14 Stat5iKO (blue) cells at d35p.i. in the spleen of LCMV Cl13 infected mice (depleted of CD4 T cells) and treated with either PBS or αPD-L1 blocking antibodies. Numbers indicate fold

changes in cell number. **G-** Representative dot plots displaying the frequency of treated (cre+, YFP$^+$) P14 WT (grey, upper panel) and P14 Stat5iKO (blue, lower panel) cells among CD8 T cells in indicated anatomical locations and experimental group at d35p.i. (F-G) Representative of 2 independent experiments with 3-5 mice/group in each.

Figure S6 (related to Figure 5): CITE-seq-mediated delineation of T_{EX} subsets A- Heatmap displaying the top representative genes per Seurat clusters (defined in **Fig. 5F**) at d27p.i. **B-** Relative distribution of indicated populations across Seurat clusters (defined in **Fig. 5F**). **C**- Number of DEGs between P14WT and P14 Stat5iKO cells in indicated mRNA-based Seurat clusters. Numbers in grey indicate DEGs with lfc≥0.25 and numbers in blue DEGs with lfc≥0.25 and P_value_adj<0.05. **D**- Detection of oligo-tagged antibodies against Ly108 and CD69 across mRNA-defined Seurat clusters (defined in **Fig. 5F**). **E**- Projection of indicated oligo-tagged antibodies-defined populations within mRNA-defined Seurat clusters (defined in **Fig. 5F**). **F-** GSEA for indicated T_{EX} subsets signature (dataset from *Beltra et. al* [27]) across indicated oligo-tagged antibodies-defined populations in P14 WT cells.

Figure S7 (related to Figure 6): Targeted delivery of IL-2/Stat5 signals using an orthogonal IL-2/IL2Rβ pair system alters T_{EX} subset dynamic at steady state and upon PD-L1 blockade. A- Absolute numbers of splenic P14 Empty^{YFP-} (grey) and P14 IL2Rβ-ortho^{YFP-} (blue) cells isolated at d26p.i. from experimental groups treated with indicated doses of *ortho*IL-2 between d21-25p.i. N=2 with 6-14 mice/group. **B-** Frequency of endogenous Tregs (CD4$^+$CD25$^+$FoxP3$^+$) in groups of LCMV Cl13 mice treated with

PBS (grey), regular IL2 (mrIL2, 25KIU,black) or *ortho*IL-2 (25KIU, blue) between d21 and 25p.i. Data were collected from the blood at d26p.i.. N=1 with 3-4 mice/group. **C-** Cumulative frequencies of indicated sub-populations among P14 Empty^{YFP+} cells isolated at d26p.i. from experimental groups infused with indicated doses of *ortho*IL-2. Dotted grey lines indicate mean frequencies of each sub-population across all experimental groups in P14 Empty^{YFP-}control cells. **D**- Cumulative frequencies of indicated sub-populations among endogenous gp33^{+} CD8 T cells isolated at d26p.i. from experimental groups infused with indicated concentrations of *ortho*IL-2. Dotted grey lines indicate mean frequencies of each sub-population across all experimental groups. (C-D) N=2 with 6-14 mice/group. **E**- UMAP of scRNAseq data combining P14 Empty^{YFP+} and P14 IL2Rβ-ortho^{YFP+} cells isolated at d26p.i. plotting Seurat clusters (**E**-left) or highlighting individual samples (**F**) and expression of representative genes per cluster (**E**-right). **G**- Relative distribution of indicated populations across Seurat clusters (defined in **Fig. S7E**). **H**- Representative contour plots of Ly108 and CD69 expression in co-transferred populations of P14 Empty^{YFP+} (grey) and P14 IL2Rβ-ortho^{YFP+} (blue) cells in indicated organs from mice treated with 250KIU of *ortho*IL-2 at d26p.i. Representative of 2 independent experiments with 2-6 mice/group. **I**- Absolute numbers of indicated populations among P14 IL2Rβ-ortho^{YFP+} cells isolated at d26p.i. from indicated experimental groups. N=2-3 independent experiments with 6-11 mice/group **J**- Frequency of YFP^{+} cells expressed as a ratio of splenic P14 IL2Rβ-ortho/P14 Empty at d26p.i. in indicated experimental groups. Representative of 2 independent experiments with 9-11 mice/group. **K**- Number of P14 Empty^{YFP+} (grey) and P14 IL2Rβ-ortho^{YFP+} (blue) per 10^6 CD8 T cells in indicated anatomical locations and experimental groups. N=1 with 3-6 mice/group.

Figure S8 (related to Figure 7): Targeted delivery of IL-2/Stat5 signals during viral rechallenge alters T_{EX} biology. A- Sorting strategy for P14 T_{MEM} (lower panel) and P14 IL2Rβ-ortho cells ($Ly108^{+}$ T_{EX} progenitors expressing the IL2Rβ-ortho receptor [YFP reporter], upper panel). **B**- Absolute numbers of indicated P14 cell populations in the spleen at d40 post re-challenge. N=1 with 3 mice/group. **C**- Heatmap for scores associated with genomic regions plotting accessibility at genomic regions identified in **Fig. 7H** for T_{EFF}, P14 Empty and P14 STAT5CA cells isolated at d8 of Cl13 infection as detailed in **Fig.3**.

Tables

Table S1: IPA results and gene input

Table S2: DAPs between P14 Empty, P14 STAT5CA and T_{EFF}

Table S3: DEGs between C2 and C3 (Fig. 4G)

Table S4: Genes with increased accessibility in P14 STAT5CA vs P14 Empty at d8p.i.

Table S5: DEGs between P14WT and P14 Stat5iKO

Table S6: DAPS between rechallenged Memory, $T_{EX}^{[PBS]}$ and $T_{EX}^{[oIL2]}$

References

1 McLane, L. M., Abdel-Hakeem, M. S. & Wherry, E. J. CD8 T Cell Exhaustion During Chronic Viral Infection and Cancer. *Annu Rev Immunol* **37**, 457-495, doi:10.1146/annurev-immunol-041015-055318 (2019).

2 Collier, J. L., Weiss, S. A., Pauken, K. E., Sen, D. R. & Sharpe, A. H. Not-so-opposite ends of the spectrum: CD8(+) T cell dysfunction across chronic infection, cancer and autoimmunity. *Nat Immunol* **22**, 809-819, doi:10.1038/s41590-021-00949-7 (2021).

3 Ramakrishna, S., Barsan, V. & Mackall, C. Prospects and challenges for use of CAR T cell therapies in solid tumors. *Expert Opin Biol Ther* **20**, 503-516, doi:10.1080/14712598.2020.1738378 (2020).

4 Wherry, E. J., Blattman, J. N., Murali-Krishna, K., van der Most, R. & Ahmed, R. Viral persistence alters CD8 T-cell immunodominance and tissue distribution and results in distinct stages of functional impairment. *J Virol* **77**, 4911-4927 (2003).

5 Zajac, A. J. *et al.* Viral immune evasion due to persistence of activated T cells without effector function. *J Exp Med* **188**, 2205-2213 (1998).

6 Yao, C. *et al.* Single-cell RNA-seq reveals TOX as a key regulator of CD8(+) T cell persistence in chronic infection. *Nat Immunol* **20**, 890-901, doi:10.1038/s41590-019-0403-4 (2019).

7 Khan, O. *et al.* TOX transcriptionally and epigenetically programs CD8(+) T cell exhaustion. *Nature* **571**, 211-218, doi:10.1038/s41586-019-1325-x (2019).

8 Alfei, F. *et al.* TOX reinforces the phenotype and longevity of exhausted T cells in chronic viral infection. *Nature* **571**, 265-269, doi:10.1038/s41586-019-1326-9 (2019).

9 Scott, A. C. *et al.* TOX is a critical regulator of tumour-specific T cell differentiation. *Nature* **571**, 270-274, doi:10.1038/s41586-019-1324-y (2019).

10 Seo, H. *et al.* TOX and TOX2 transcription factors cooperate with NR4A transcription factors to impose CD8(+) T cell exhaustion. *Proc Natl Acad Sci U S A* **116**, 12410-12415, doi:10.1073/pnas.1905675116 (2019).

11 Abdel-Hakeem, M. S. *et al.* Epigenetic scarring of exhausted T cells hinders memory differentiation upon eliminating chronic antigenic stimulation. *Nat Immunol* **22**, 1008-1019, doi:10.1038/s41590-021-00975-5 (2021).

12 Tonnerre, P. *et al.* Differentiation of exhausted CD8(+) T cells after termination of chronic antigen stimulation stops short of achieving functional T cell memory. *Nat Immunol* **22**, 1030-1041, doi:10.1038/s41590-021-00982-6 (2021).

13 Yates, K. B. *et al.* Epigenetic scars of CD8(+) T cell exhaustion persist after cure of chronic infection in humans. *Nat Immunol* **22**, 1020-1029, doi:10.1038/s41590-021-00979-1 (2021).

14 Angelosanto, J. M., Blackburn, S. D., Crawford, A. & Wherry, E. J. Progressive loss of memory T cell potential and commitment to exhaustion during chronic viral infection. *J Virol* **86**, 8161-8170, doi:JVI.00889-12 [pii]
10.1128/JVI.00889-12 (2012).

15 West, E. E. *et al.* Tight regulation of memory CD8(+) T cells limits their effectiveness during sustained high viral load. *Immunity* **35**, 285-298, doi:10.1016/j.immuni.2011.05.017 (2011).

16 Cartwright, E. K. *et al.* CD8(+) Lymphocytes Are Required for Maintaining Viral Suppression in SIV-Infected Macaques Treated with Short-Term Antiretroviral Therapy. *Immunity* **45**, 656-668, doi:10.1016/j.immuni.2016.08.018 (2016).

17 Mueller, Y. M. *et al.* CD8+ cell depletion of SHIV89.6P-infected macaques induces CD4+ T cell proliferation that contributes to increased viral loads. *J Immunol* **183**, 5006-5012, doi:10.4049/jimmunol.0900141 (2009).

18 Jin, X. *et al.* Dramatic rise in plasma viremia after CD8(+) T cell depletion in simian immunodeficiency virus-infected macaques. *J Exp Med* **189**, 991-998, doi:10.1084/jem.189.6.991 (1999).

19 Ribas, A. & Wolchok, J. D. Cancer immunotherapy using checkpoint blockade. *Science* **359**, 1350-1355, doi:10.1126/science.aar4060 (2018).

20 Huang, A. C. *et al.* T-cell invigoration to tumour burden ratio associated with anti-PD-1 response. *Nature* **545**, 60-65, doi:10.1038/nature22079 (2017).

21 Li, H. *et al.* Dysfunctional CD8 T Cells Form a Proliferative, Dynamically Regulated Compartment within Human Melanoma. *Cell* **181**, 747, doi:10.1016/j.cell.2020.04.017 (2020).

22 Kamphorst, A. O. *et al.* Rescue of exhausted CD8 T cells by PD-1-targeted therapies is CD28-dependent. *Science* **355**, 1423-1427, doi:10.1126/science.aaf0683 (2017).

23 Sade-Feldman, M. *et al.* Defining T Cell States Associated with Response to Checkpoint Immunotherapy in Melanoma. *Cell* **175**, 998-1013 e1020, doi:10.1016/j.cell.2018.10.038 (2018).

24 Cercek, A. *et al.* PD-1 Blockade in Mismatch Repair-Deficient, Locally Advanced Rectal Cancer. *N Engl J Med*, doi:10.1056/NEJMoa2201445 (2022).

25 Pauken, K. E. *et al.* Epigenetic stability of exhausted T cells limits durability of reinvigoration by PD-1 blockade. *Science*, doi:10.1126/science.aaf2807 (2016).

26 Giles, J. R. *et al.* Longitudinal single cell transcriptional and epigenetic mapping of effector, memory, and exhausted CD8 T cells reveals shared biological circuits across distinct cell fates. *bioRxiv*, 2022.2003.2027.485974, doi:10.1101/2022.03.27.485974 (2022).

27 Beltra, J. C. *et al.* Developmental Relationships of Four Exhausted CD8(+) T Cell Subsets Reveals Underlying Transcriptional and Epigenetic Landscape Control Mechanisms. *Immunity* **52**, 825-841 e828, doi:10.1016/j.immuni.2020.04.014 (2020).

28 Hudson, W. H. *et al.* Proliferating Transitory T Cells with an Effector-like Transcriptional Signature Emerge from PD-1(+) Stem-like CD8(+) T Cells during Chronic Infection. *Immunity* **51**, 1043-1058 e1044, doi:10.1016/j.immuni.2019.11.002 (2019).

29 Zander, R. *et al.* CD4(+) T Cell Help Is Required for the Formation of a Cytolytic CD8(+) T Cell Subset that Protects against Chronic Infection and Cancer. *Immunity* **51**, 1028-1042 e1024, doi:10.1016/j.immuni.2019.10.009 (2019).

30 Sandu, I. *et al.* Landscape of Exhausted Virus-Specific CD8 T Cells in Chronic LCMV Infection. *Cell Rep* **32**, 108078, doi:10.1016/j.celrep.2020.108078 (2020).

31 Im, S. J. *et al.* Defining CD8+ T cells that provide the proliferative burst after PD-1 therapy. *Nature* **537**, 417-421, doi:10.1038/nature19330 (2016).

32 Utzschneider, D. T. *et al.* T Cell Factor 1-Expressing Memory-like CD8(+) T Cells Sustain the Immune Response to Chronic Viral Infections. *Immunity* **45**, 415-427, doi:10.1016/j.immuni.2016.07.021 (2016).

33 Wu, T. *et al.* The TCF1-Bcl6 axis counteracts type I interferon to repress exhaustion and maintain T cell stemness. *Sci Immunol* **1**, doi:10.1126/sciimmunol.aai8593 (2016).

34 Zhang, K., Wang, M., Zhao, Y. & Wang, W. Taiji: System-level identification of key transcription factors reveals transcriptional waves in mouse embryonic development. *Sci Adv* **5**, eaav3262, doi:10.1126/sciadv.aav3262 (2019).

35 Chen, Z. *et al.* TCF-1-Centered Transcriptional Network Drives an Effector versus Exhausted CD8 T Cell-Fate Decision. *Immunity* **51**, 840-855 e845, doi:10.1016/j.immuni.2019.09.013 (2019).

36 Hand, T. W. *et al.* Differential effects of STAT5 and PI3K/AKT signaling on effector and memory CD8 T-cell survival. *Proc Natl Acad Sci U S A* **107**, 16601-16606, doi:10.1073/pnas.1003457107 (2010).

37 Onishi, M. *et al.* Identification and characterization of a constitutively active STAT5 mutant that promotes cell proliferation. *Mol Cell Biol* **18**, 3871-3879, doi:10.1128/MCB.18.7.3871 (1998).

38 Tripathi, P. *et al.* STAT5 is critical to maintain effector CD8+ T cell responses. *J Immunol* **185**, 2116-2124, doi:10.4049/jimmunol.1000842 (2010).

39 Mitchell, D. M. & Williams, M. A. Disparate roles for STAT5 in primary and secondary CTL responses. *J Immunol* **190**, 3390-3398, doi:10.4049/jimmunol.1202674 (2013).

40 Sen, D. R. *et al.* The epigenetic landscape of T cell exhaustion. *Science*, doi:10.1126/science.aae0491 (2016).

41 Buenrostro, J. D., Giresi, P. G., Zaba, L. C., Chang, H. Y. & Greenleaf, W. J. Transposition of native chromatin for fast and sensitive epigenomic profiling of open chromatin, DNA-binding proteins and nucleosome position. *Nat Methods* **10**, 1213-1218, doi:10.1038/nmeth.2688 (2013).

42 Martinez, G. J. *et al.* The transcription factor NFAT promotes exhaustion of activated CD8(+) T cells. *Immunity* **42**, 265-278, doi:10.1016/j.immuni.2015.01.006 (2015).

43 Klein-Hessling, S. *et al.* NFATc1 controls the cytotoxicity of CD8(+) T cells. *Nat Commun* **8**, 511, doi:10.1038/s41467-017-00612-6 (2017).

44 Daniel, B. *et al.* Divergent clonal differentiation trajectories of T cell exhaustion. *bioRxiv*, 2021.2012.2016.472900, doi:10.1101/2021.12.16.472900 (2021).

45 Odorizzi, P. M., Pauken, K. E., Paley, M. A., Sharpe, A. & Wherry, E. J. Genetic absence of PD-1 promotes accumulation of terminally differentiated exhausted CD8+ T cells. *J Exp Med* **212**, 1125-1137, doi:10.1084/jem.20142237 (2015).

46 Blattman, J. N., Wherry, E. J., Ha, S. J., van der Most, R. G. & Ahmed, R. Impact of epitope escape on PD-1 expression and CD8 T-cell exhaustion during chronic infection. *J Virol* **83**, 4386-4394, doi:10.1128/JVI.02524-08 (2009).

47 Sockolosky, J. T. *et al.* Selective targeting of engineered T cells using orthogonal IL-2 cytokine-receptor complexes. *Science* **359**, 1037-1042, doi:10.1126/science.aar3246 (2018).

48 West, E. E. *et al.* PD-L1 blockade synergizes with IL-2 therapy in reinvigorating exhausted T cells. *J Clin Invest* **123**, 2604-2615, doi:67008 [pii]
10.1172/JCI67008 (2013).

49 Zhou, X. *et al.* Differentiation and persistence of memory CD8(+) T cells depend on T cell factor 1. *Immunity* **33**, 229-240, doi:10.1016/j.immuni.2010.08.002 (2010).

50 Delpoux, A., Lai, C. Y., Hedrick, S. M. & Doedens, A. L. FOXO1 opposition of CD8(+) T cell effector programming confers early memory properties and phenotypic diversity. *Proc Natl Acad Sci U S A* **114**, E8865-E8874, doi:10.1073/pnas.1618916114 (2017).

51 Shan, Q. *et al.* Tcf1 and Lef1 provide constant supervision to mature CD8(+) T cell identity and function by organizing genomic architecture. *Nat Commun* **12**, 5863, doi:10.1038/s41467-021-26159-1 (2021).

52 Doering, T. A. *et al.* Network Analysis Reveals Centrally Connected Genes and Pathways Involved in CD8(+) T Cell Exhaustion versus Memory. *Immunity* **37**, 1130-1144, doi:S1074-7613(12)00470-0 [pii]
10.1016/j.immuni.2012.08.021 (2012).

53 Delgoffe, G. M. *et al.* The role of exhaustion in CAR T cell therapy. *Cancer Cell* **39**, 885-888, doi:10.1016/j.ccell.2021.06.012 (2021).

54 Blattman, J. N. *et al.* Therapeutic use of IL-2 to enhance antiviral T-cell responses in vivo. *Nat Med* **9**, 540-547, doi:10.1038/nm866
nm866 [pii] (2003).

55 Rosenberg, S. A. IL-2: the first effective immunotherapy for human cancer. *J Immunol* **192**, 5451-5458, doi:10.4049/jimmunol.1490019 (2014).

56 Beltra, J. C. *et al.* IL2Rbeta-dependent signals drive terminal exhaustion and suppress memory development during chronic viral infection. *Proc Natl Acad Sci U S A* **113**, E5444-5453, doi:10.1073/pnas.1604256113 (2016).

57 Shan, Q. *et al.* Ectopic Tcf1 expression instills a stem-like program in exhausted CD8(+) T cells to enhance viral and tumor immunity. *Cell Mol Immunol* **18**, 1262-1277, doi:10.1038/s41423-020-0436-5 (2021).

58 Mo, F. *et al.* An engineered IL-2 partial agonist promotes CD8(+) T cell stemness. *Nature* **597**, 544-548, doi:10.1038/s41586-021-03861-0 (2021).

59 Hinrichs, C. S. *et al.* IL-2 and IL-21 confer opposing differentiation programs to CD8+ T cells for adoptive immunotherapy. *Blood* **111**, 5326-5333, doi:blood-2007-09-113050 [pii]
10.1182/blood-2007-09-113050 (2008).

60 Grange, M. *et al.* Active STAT5 regulates T-bet and eomesodermin expression in CD8 T cells and imprints a T-bet-dependent Tc1 program with repressed IL-6/TGF-beta1 signaling. *J Immunol* **191**, 3712-3724, doi:10.4049/jimmunol.1300319 (2013).

61 Kalbasi, A. *et al.* Potentiating adoptive cell therapy using synthetic IL-9 receptors. *Nature* **607**, 360-365, doi:10.1038/s41586-022-04801-2 (2022).

62 Utzschneider, D. T. *et al.* Early precursor T cells establish and propagate T cell exhaustion in chronic infection. *Nat Immunol* **21**, 1256-1266, doi:10.1038/s41590-020-0760-z (2020).

63 Danilo, M., Chennupati, V., Silva, J. G., Siegert, S. & Held, W. Suppression of Tcf1 by Inflammatory Cytokines Facilitates Effector CD8 T Cell Differentiation. *Cell Rep* **22**, 2107-2117, doi:10.1016/j.celrep.2018.01.072 (2018).

64 Wherry, E. J., Barber, D. L., Kaech, S. M., Blattman, J. N. & Ahmed, R. Antigen-independent memory CD8 T cells do not develop during chronic viral infection. *Proc Natl Acad Sci U S A* **101**, 16004-16009, doi:0407192101 [pii]
10.1073/pnas.0407192101 (2004).

65 Shin, H., Blackburn, S. D., Blattman, J. N. & Wherry, E. J. Viral antigen and extensive division maintain virus-specific CD8 T cells during chronic infection. *J Exp Med* **204**, 941-949, doi:jem.20061937 [pii]
10.1084/jem.20061937 (2007).
66 Siddiqui, I. *et al.* Intratumoral Tcf1(+)PD-1(+)CD8(+) T Cells with Stem-like Properties Promote Tumor Control in Response to Vaccination and Checkpoint Blockade Immunotherapy. *Immunity* **50**, 195-211 e110, doi:10.1016/j.immuni.2018.12.021 (2019).
67 Williams, M. A., Tyznik, A. J. & Bevan, M. J. Interleukin-2 signals during priming are required for secondary expansion of CD8+ memory T cells. *Nature* **441**, 890-893, doi:nature04790 [pii]
10.1038/nature04790 (2006).
68 Pipkin, M. E. *et al.* Interleukin-2 and inflammation induce distinct transcriptional programs that promote the differentiation of effector cytolytic T cells. *Immunity* **32**, 79-90, doi:S1074-7613(10)00010-5 [pii]
10.1016/j.immuni.2009.11.012 (2010).
69 Kalia, V. *et al.* Prolonged interleukin-2Ralpha expression on virus-specific CD8+ T cells favors terminal-effector differentiation in vivo. *Immunity* **32**, 91-103, doi:S1074-7613(10)00008-7 [pii]
10.1016/j.immuni.2009.11.010 (2010).
70 Mathieu, C. *et al.* IL-2 and IL-15 regulate CD8+ memory T-cell differentiation but are dispensable for protective recall responses. *Eur J Immunol* **45**, 3324-3338, doi:10.1002/eji.201546000 (2015).
71 Boulet, S., Daudelin, J. F. & Labrecque, N. IL-2 Induction of Blimp-1 Is a Key In Vivo Signal for CD8+ Short-Lived Effector T Cell Differentiation. *J Immunol*, doi:10.4049/jimmunol.1302365 (2014).
72 Mitchell, D. M., Ravkov, E. V. & Williams, M. A. Distinct roles for IL-2 and IL-15 in the differentiation and survival of CD8+ effector and memory T cells. *J Immunol* **184**, 6719-6730, doi:jimmunol.0904089 [pii]
10.4049/jimmunol.0904089 (2010).
73 Liao, W., Lin, J. X. & Leonard, W. J. Interleukin-2 at the crossroads of effector responses, tolerance, and immunotherapy. *Immunity* **38**, 13-25, doi:10.1016/j.immuni.2013.01.004 (2013).
74 Spolski, R., Li, P. & Leonard, W. J. Biology and regulation of IL-2: from molecular mechanisms to human therapy. *Nat Rev Immunol* **18**, 648-659, doi:10.1038/s41577-018-0046-y (2018).
75 Shourian, M., Beltra, J. C., Bourdin, B. & Decaluwe, H. Common gamma chain cytokines and CD8 T cells in cancer. *Semin Immunol* **42**, 101307, doi:10.1016/j.smim.2019.101307 (2019).
76 Gattinoni, L. *et al.* Wnt signaling arrests effector T cell differentiation and generates CD8+ memory stem cells. *Nat Med* **15**, 808-813, doi:10.1038/nm.1982 (2009).
77 Shin, H. M. *et al.* Epigenetic modifications induced by Blimp-1 Regulate CD8(+) T cell memory progression during acute virus infection. *Immunity* **39**, 661-675, doi:10.1016/j.immuni.2013.08.032 (2013).

78 Gong, D. & Malek, T. R. Cytokine-dependent Blimp-1 expression in activated T cells inhibits IL-2 production. *J Immunol* **178**, 242-252, doi:178/1/242 [pii] (2007).

79 Martins, G. A., Cimmino, L., Liao, J., Magnusdottir, E. & Calame, K. Blimp-1 directly represses Il2 and the Il2 activator Fos, attenuating T cell proliferation and survival. *J Exp Med* **205**, 1959-1965, doi:10.1084/jem.20080526 (2008).

80 Welsh, R. M. & Seedhom, M. O. Lymphocytic choriomeningitis virus (LCMV): propagation, quantitation, and storage. *Curr Protoc Microbiol* **Chapter 15**, Unit 15A 11, doi:10.1002/9780471729259.mc15a01s8 (2008).

81 Kurachi, M. *et al.* Optimized retroviral transduction of mouse T cells for in vivo assessment of gene function. *Nat Protoc* **12**, 1980-1998, doi:10.1038/nprot.2017.083 (2017).

82 Skene, P. J., Henikoff, J. G. & Henikoff, S. Targeted in situ genome-wide profiling with high efficiency for low cell numbers. *Nat Protoc* **13**, 1006-1019, doi:10.1038/nprot.2018.015 (2018).

83 Cao, Z. *et al.* ZMYND8-regulated IRF8 transcription axis is an acute myeloid leukemia dependency. *Mol Cell* **81**, 3604-3622 e3610, doi:10.1016/j.molcel.2021.07.018 (2021).

84 Villarino, A. V. *et al.* Subset- and tissue-defined STAT5 thresholds control homeostasis and function of innate lymphoid cells. *J Exp Med* **214**, 2999-3014, doi:10.1084/jem.20150907 (2017).

85 Butler, A., Hoffman, P., Smibert, P., Papalexi, E. & Satija, R. Integrating single-cell transcriptomic data across different conditions, technologies, and species. *Nat Biotechnol* **36**, 411-420, doi:10.1038/nbt.4096 (2018).

Figure. 1

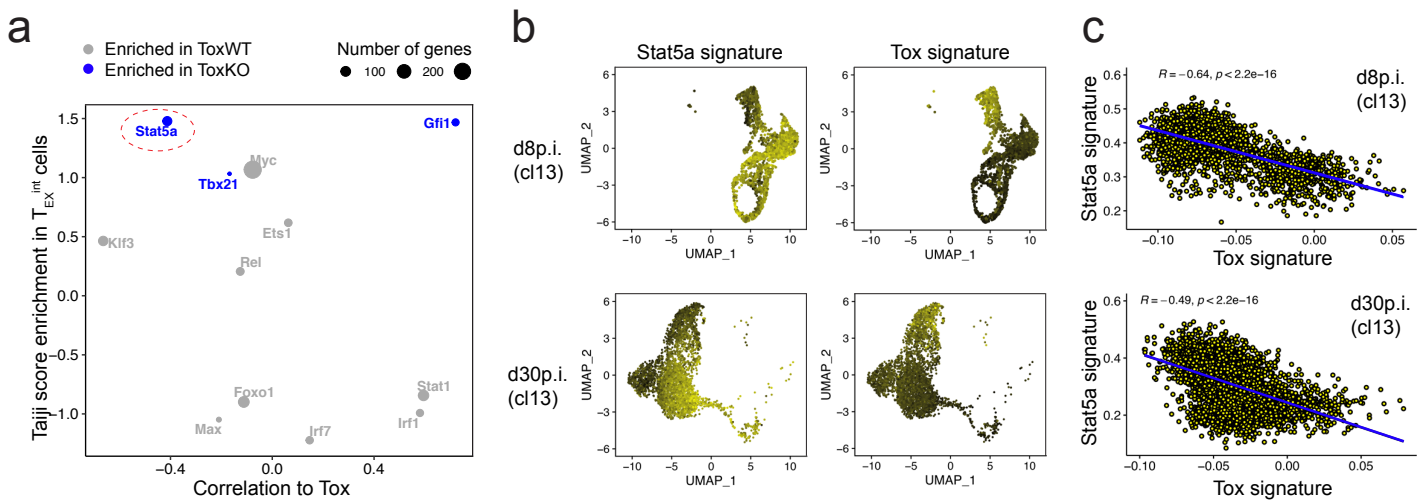

Figure 2

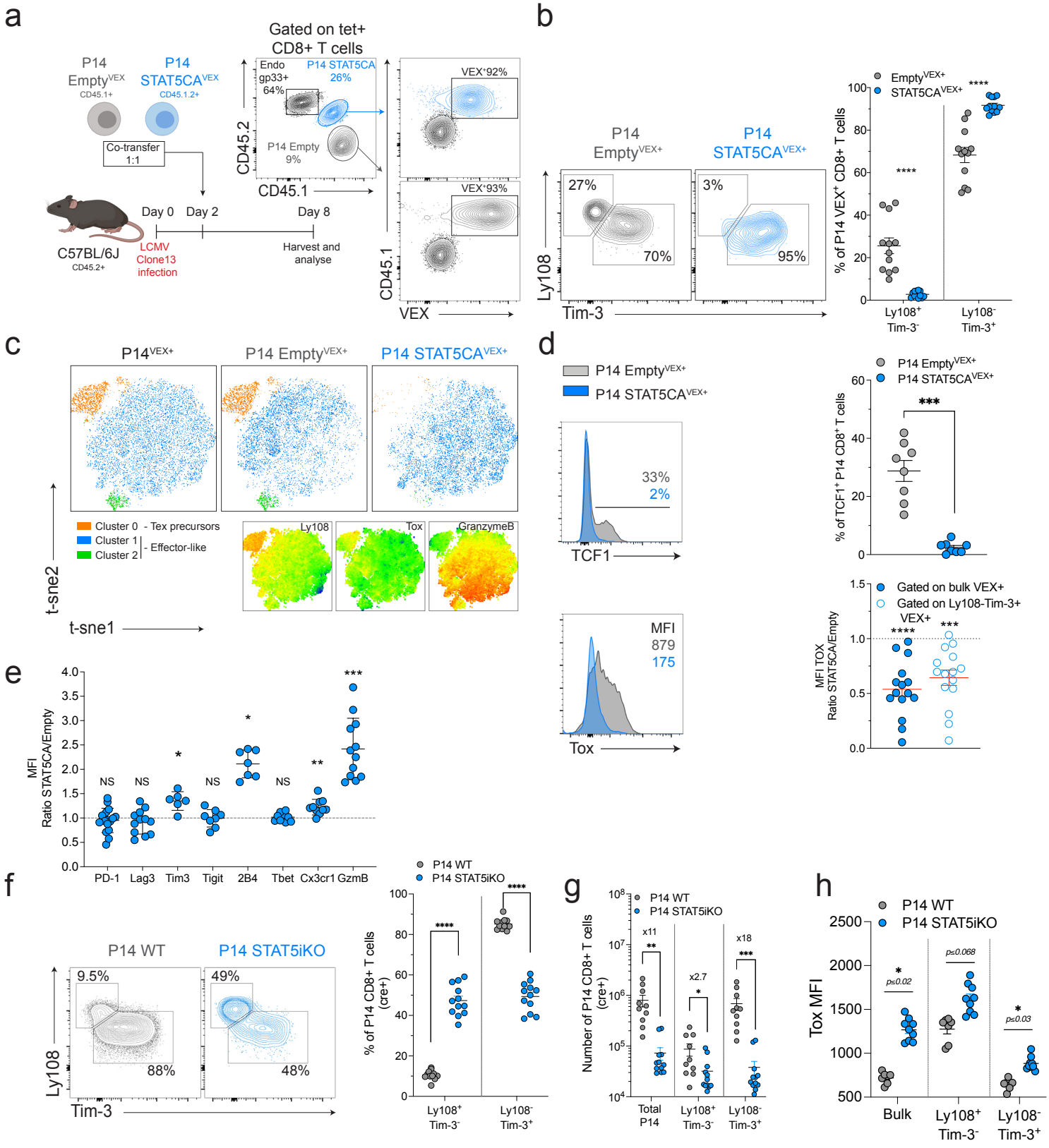

Figure. 3

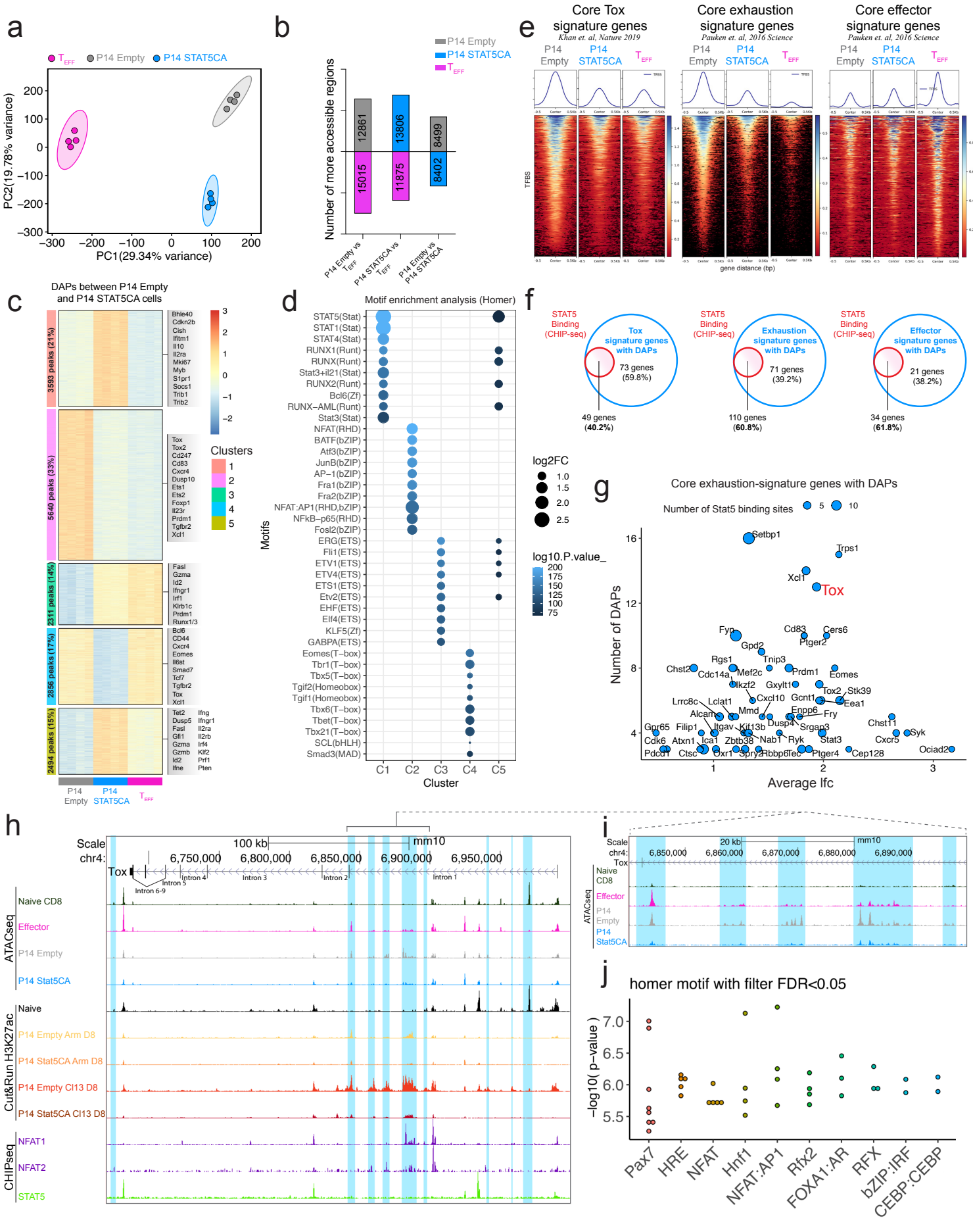

Figure 4

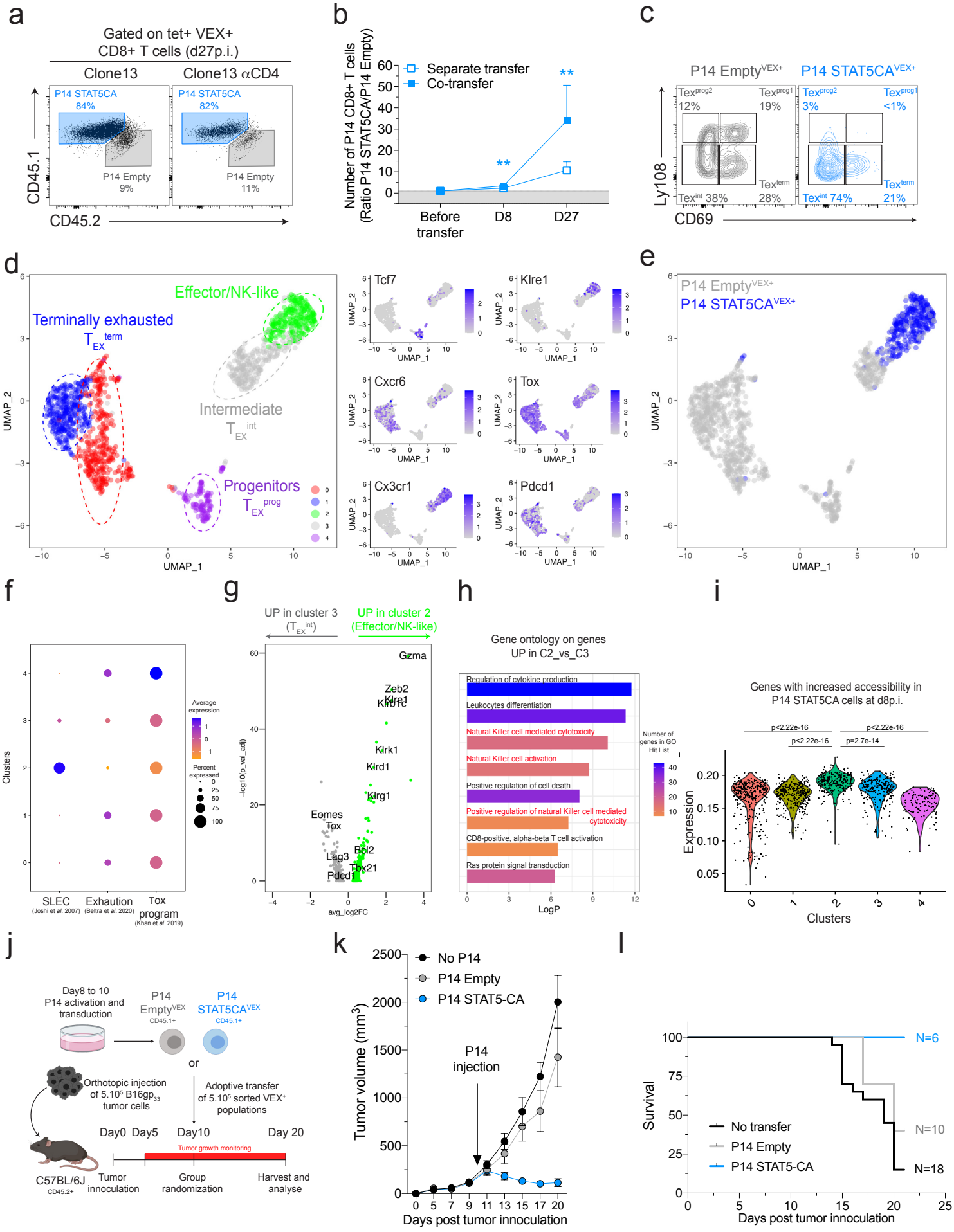

Figure 5

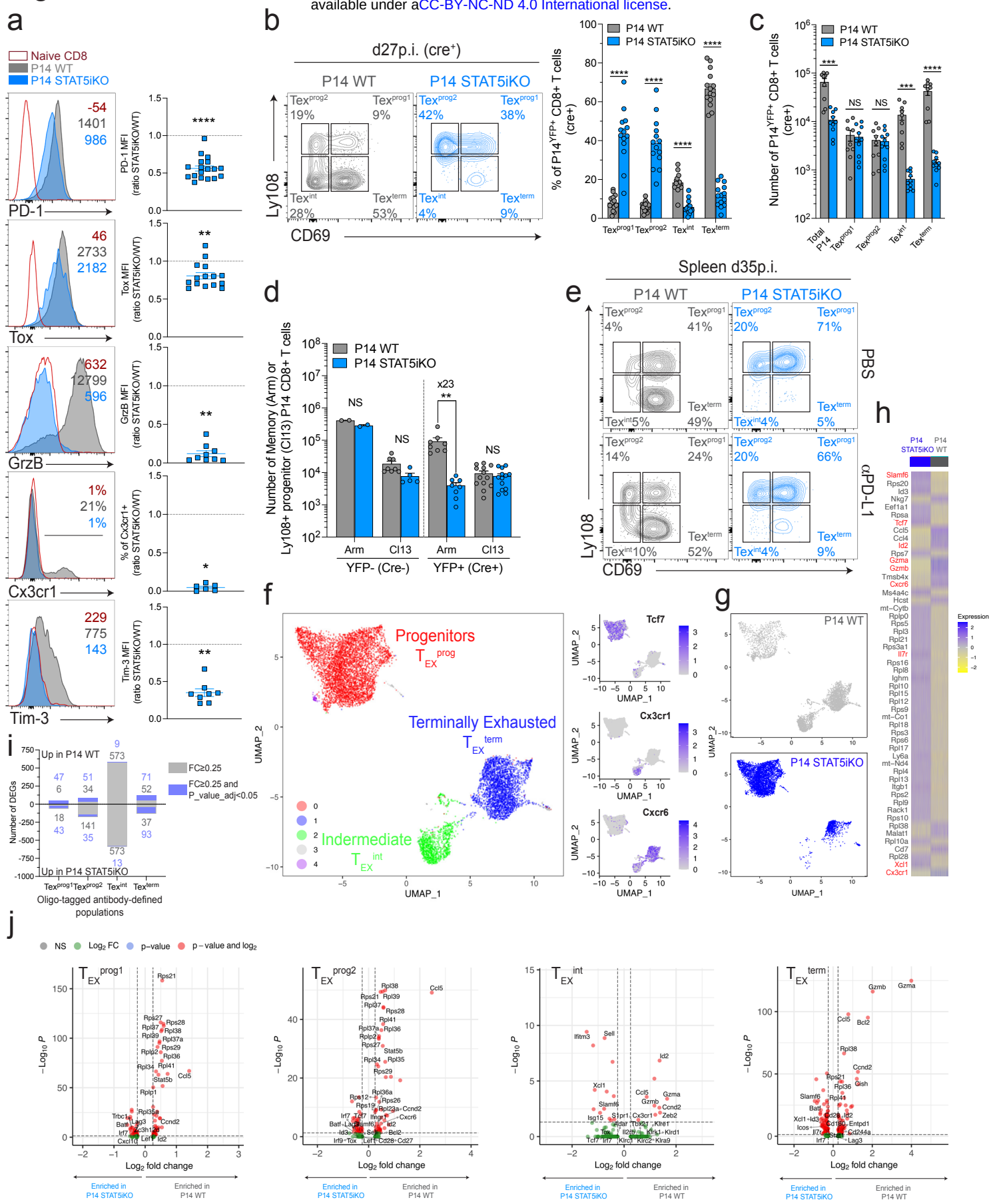

Figure 6

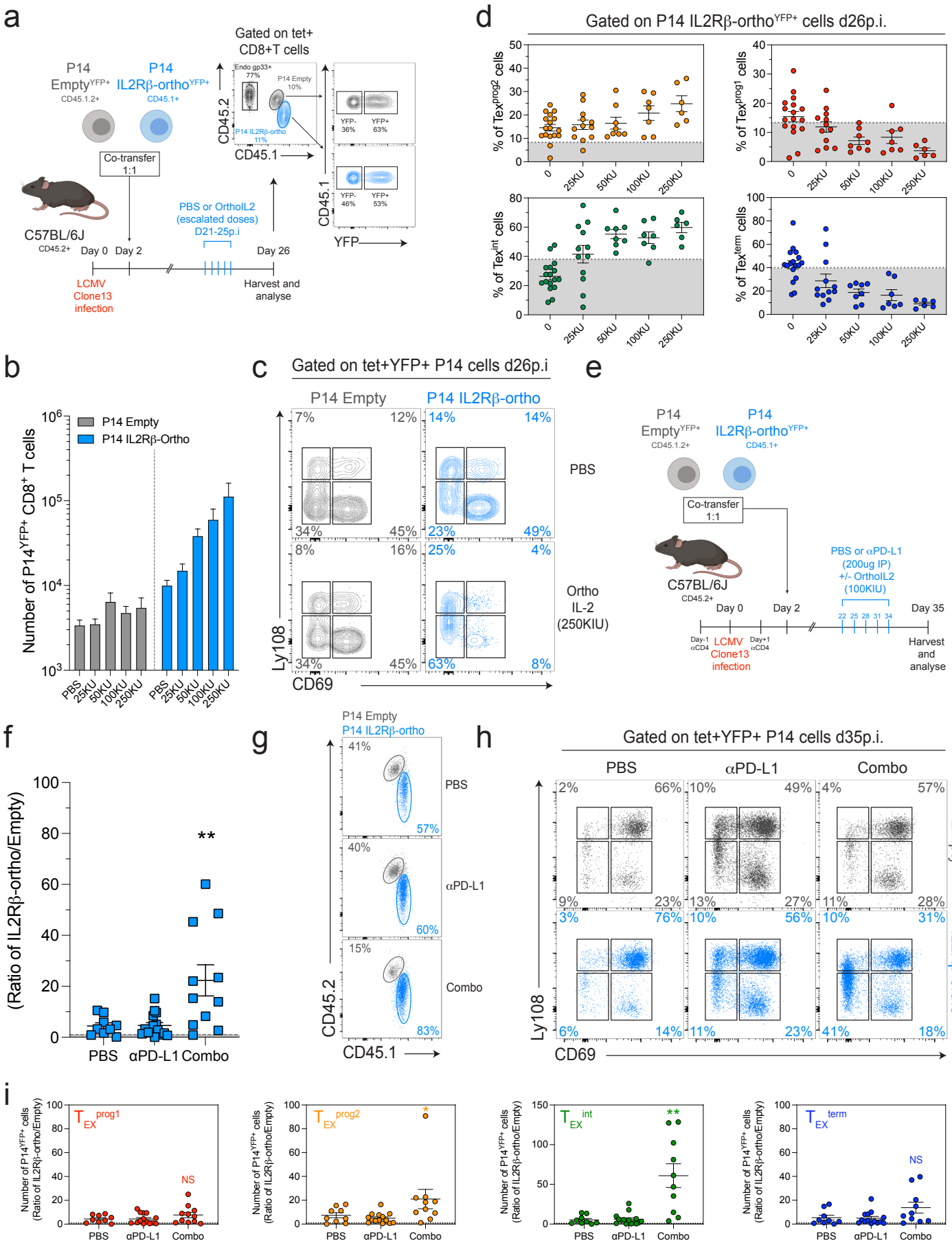

Figure: 7

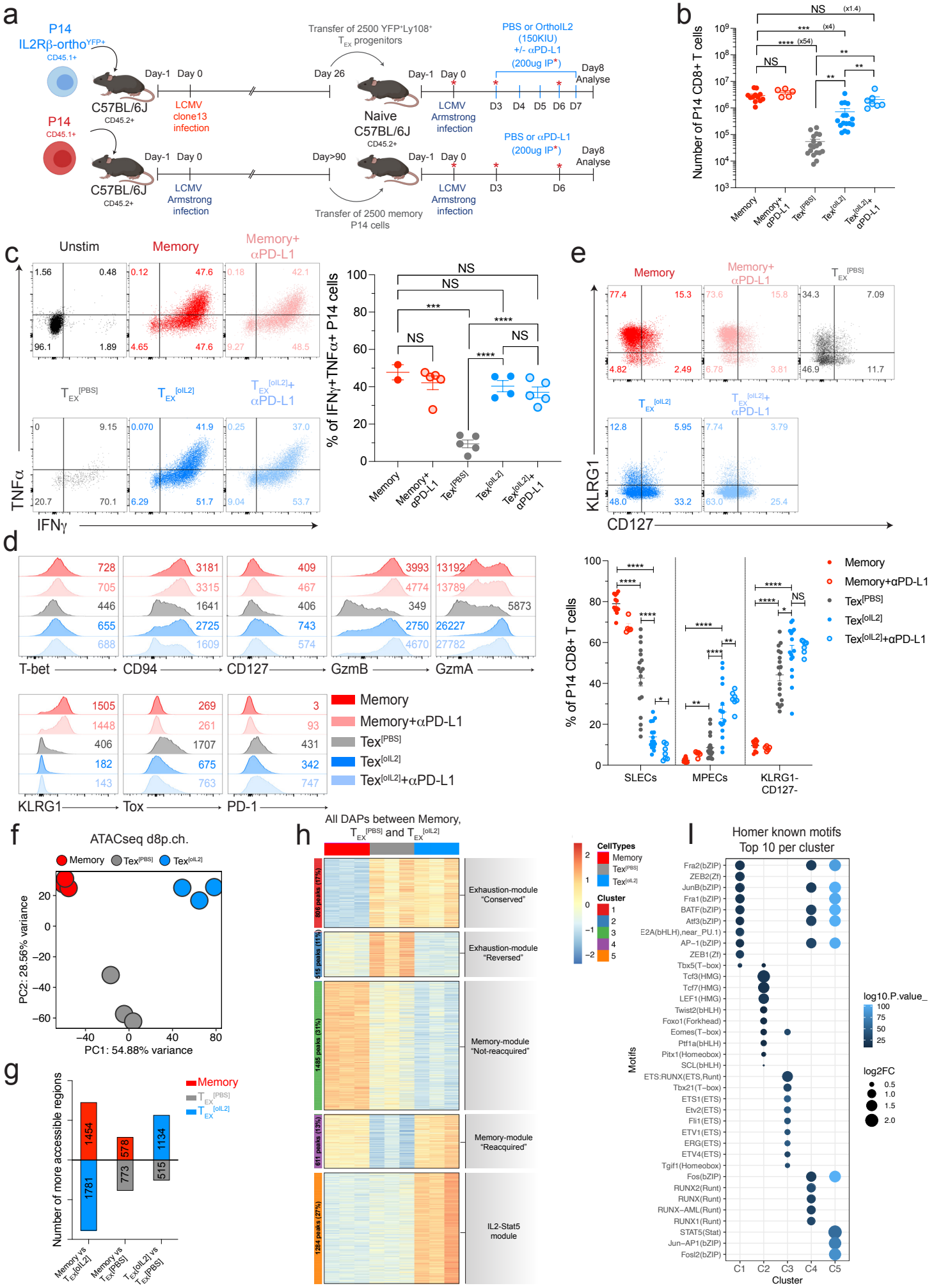

Figure: S1

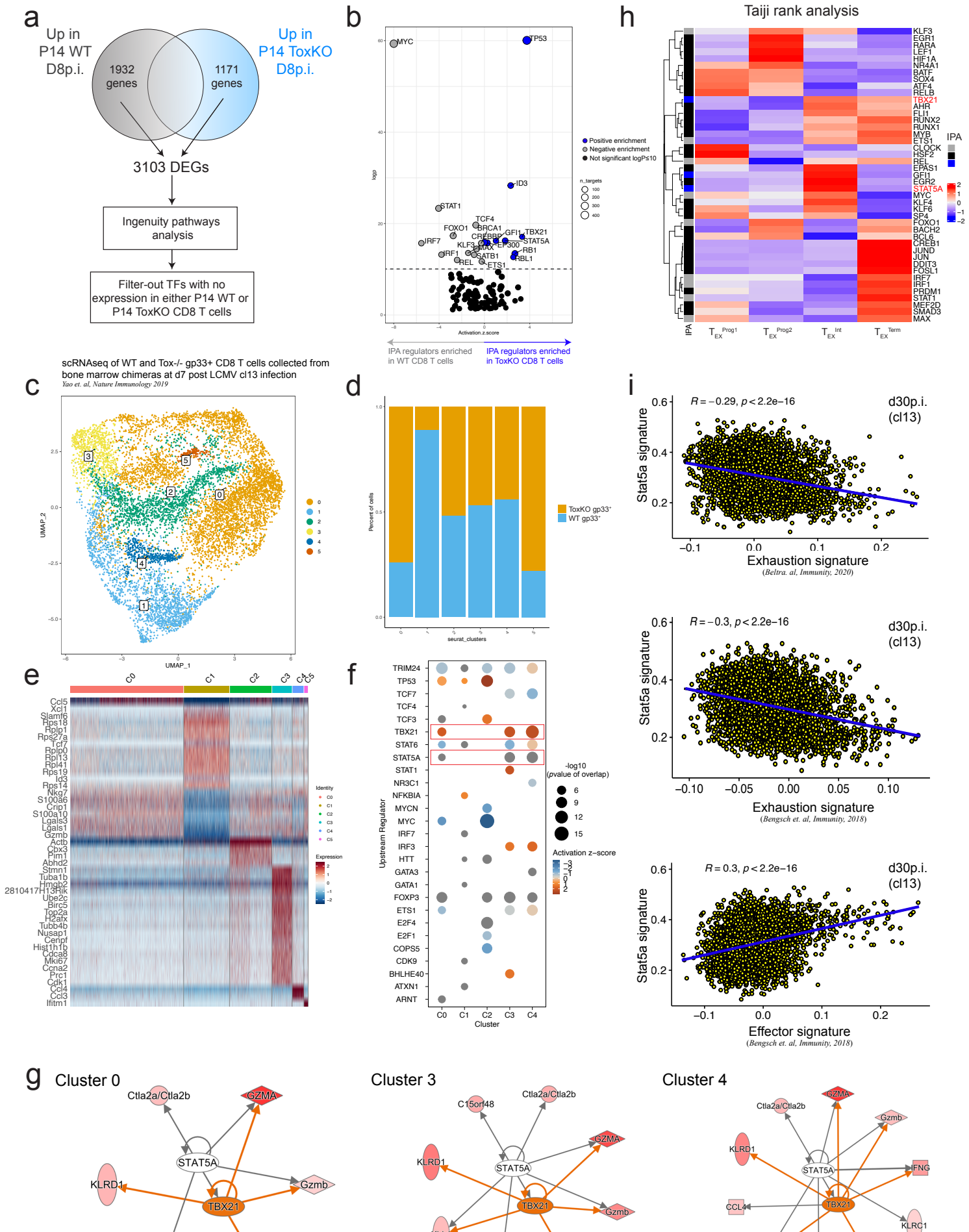

Figure S2

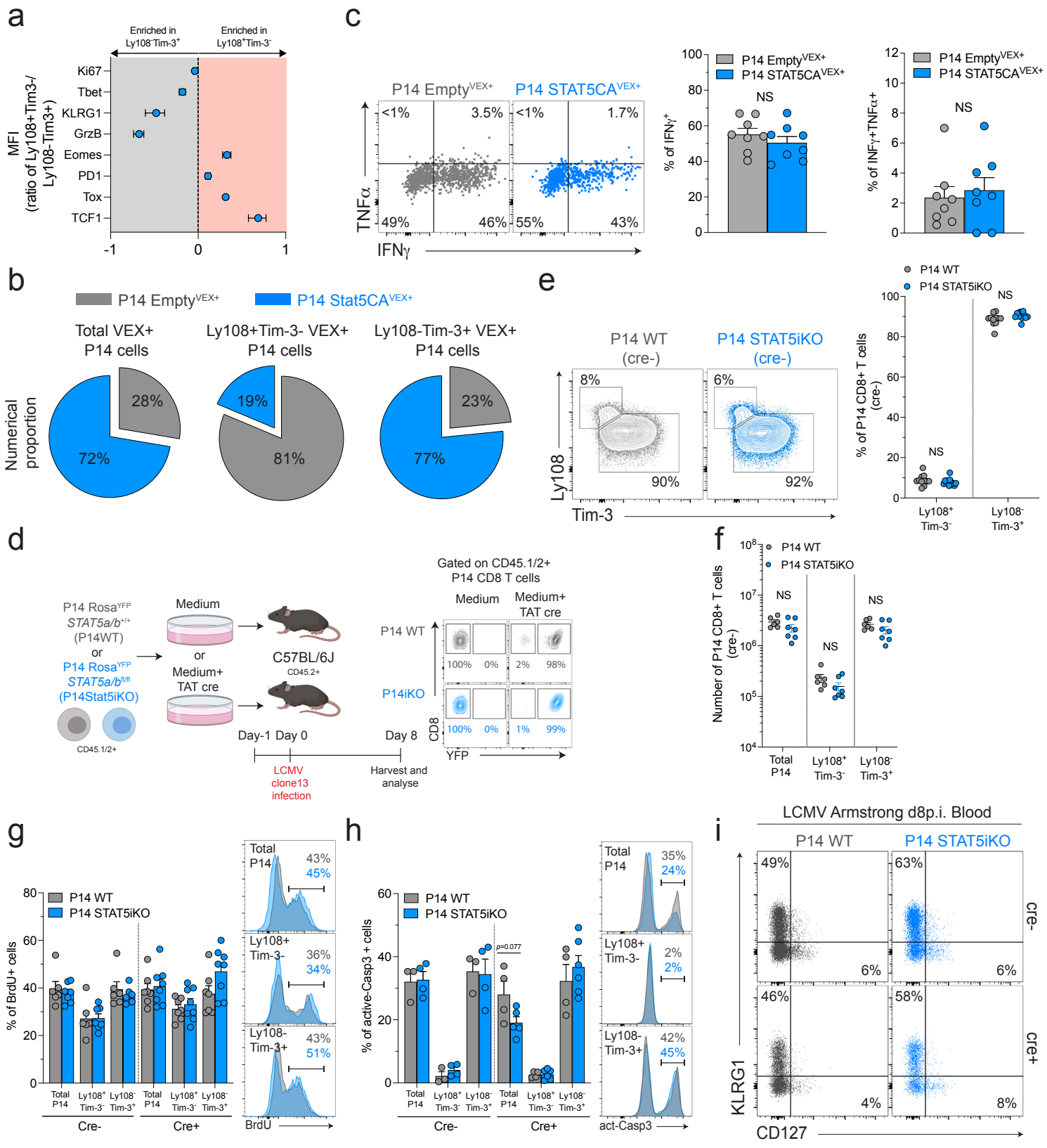

Figure S3

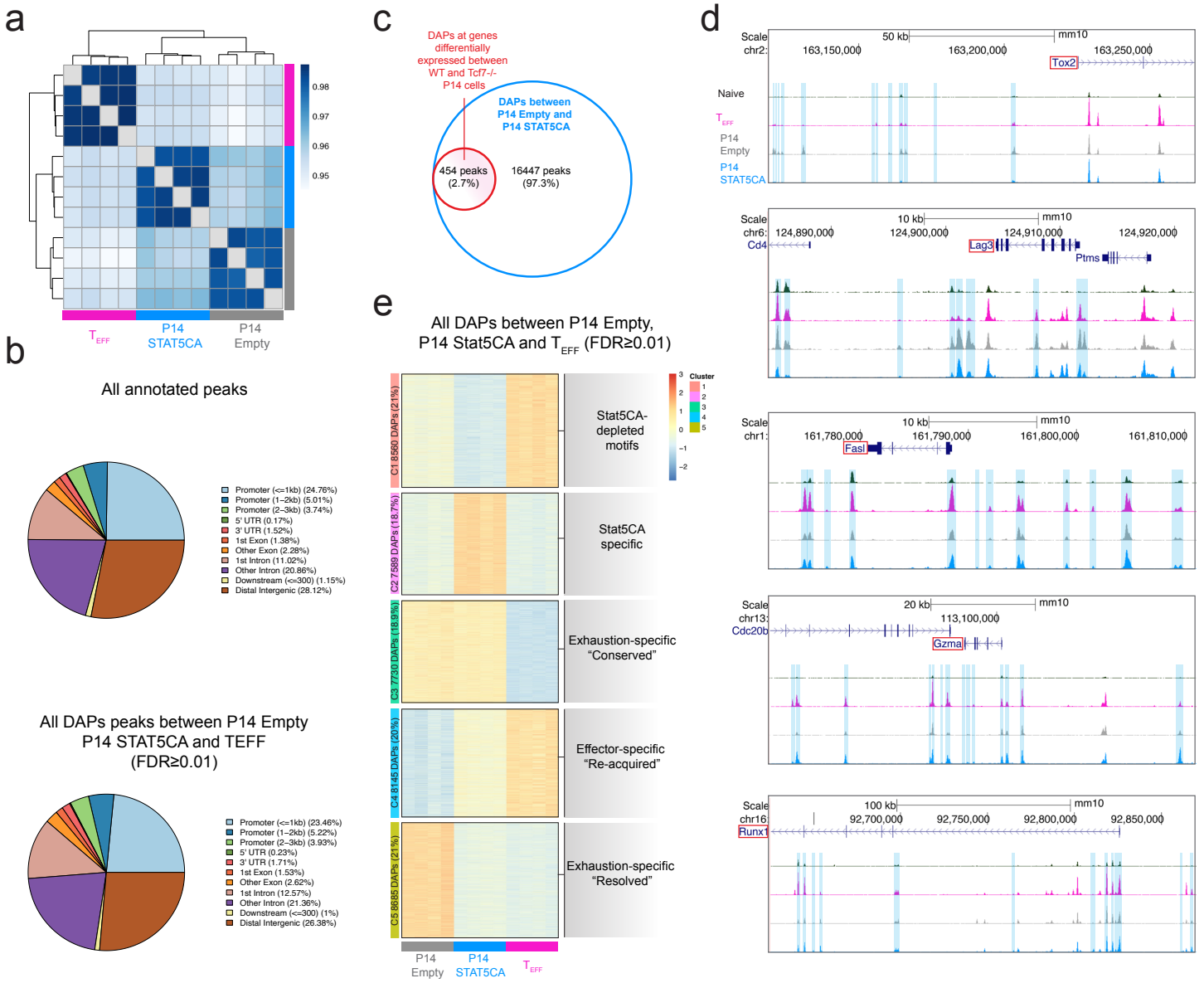

Figure. S4

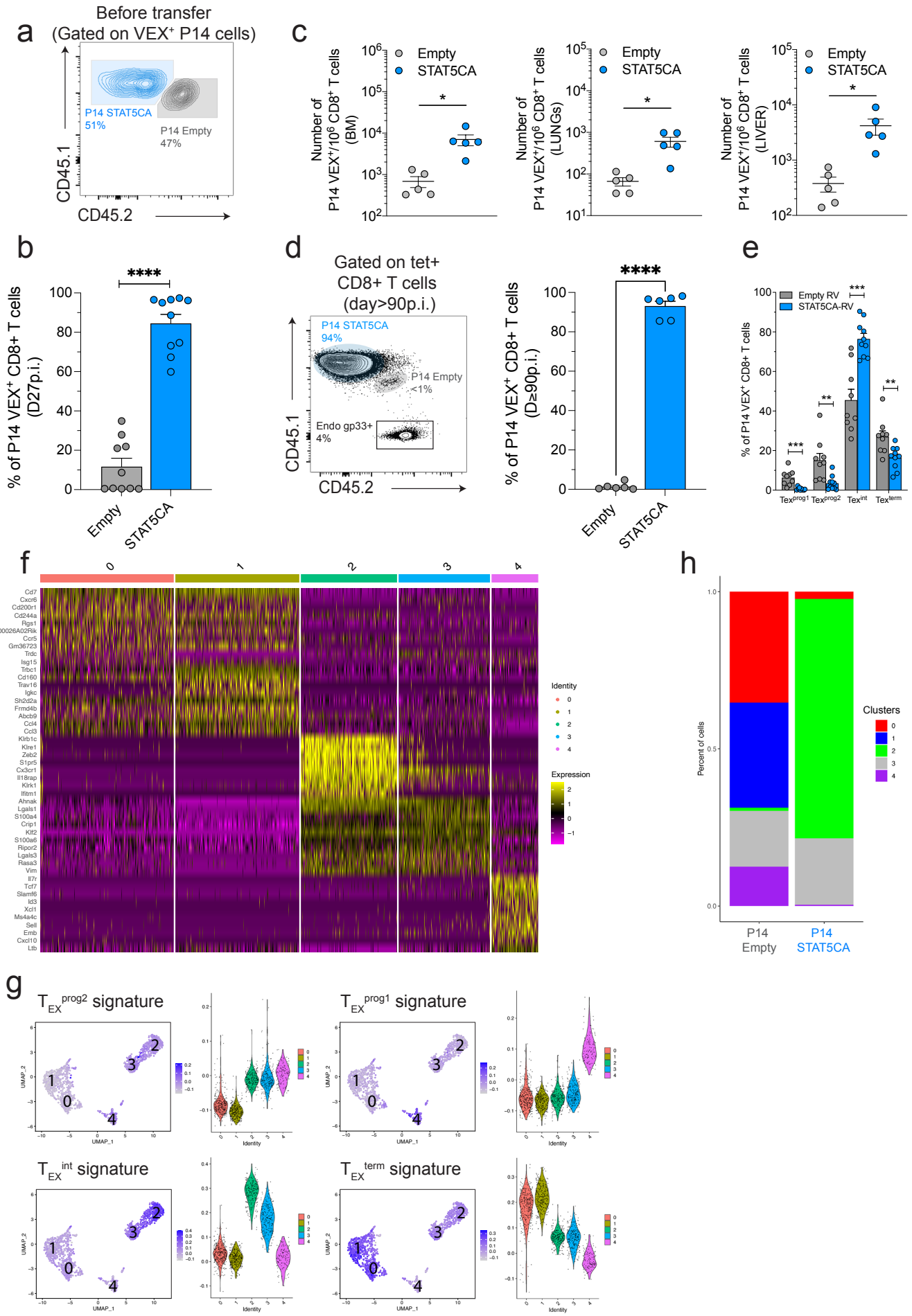

Figure. S5

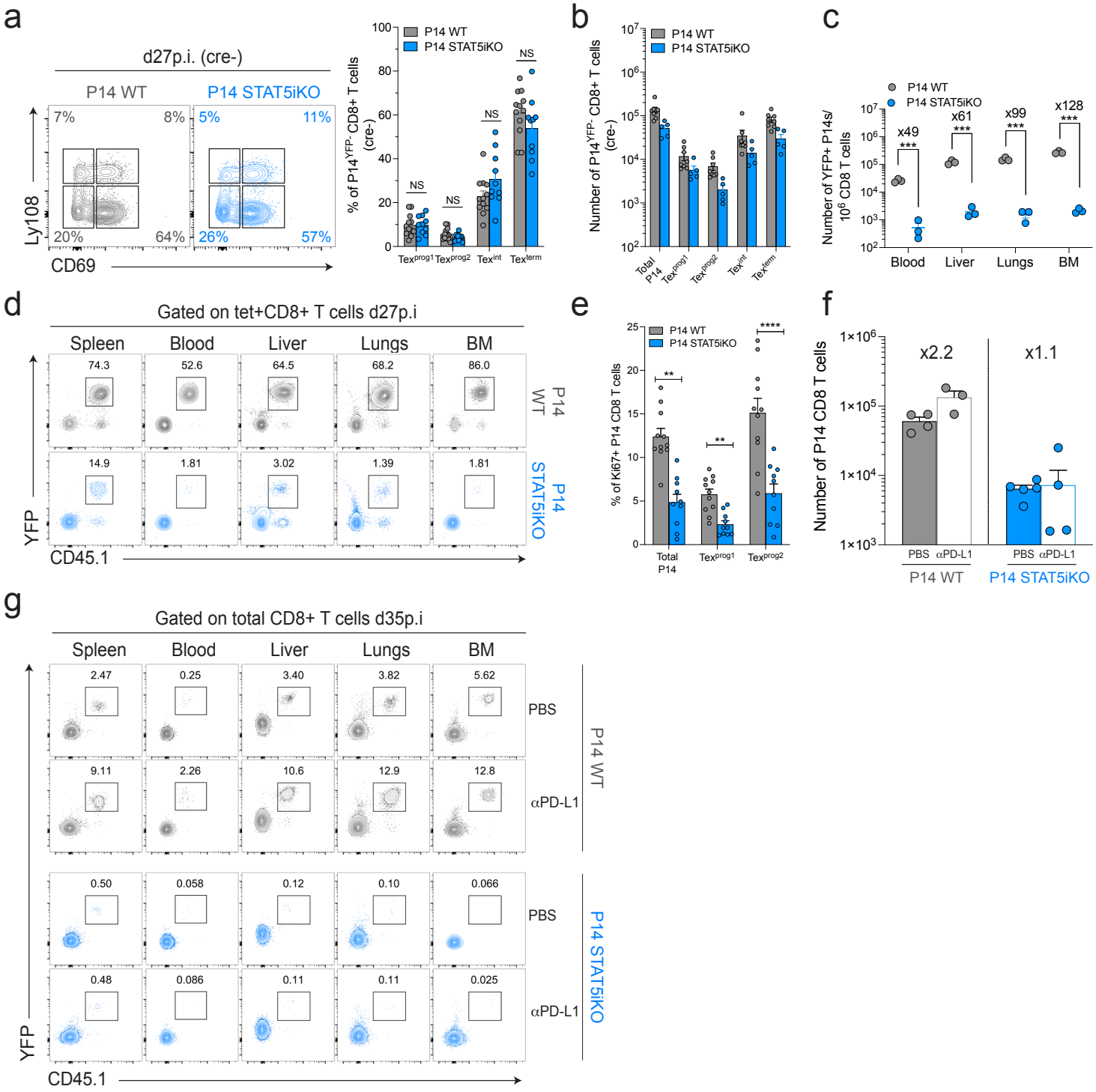

Figure. S6

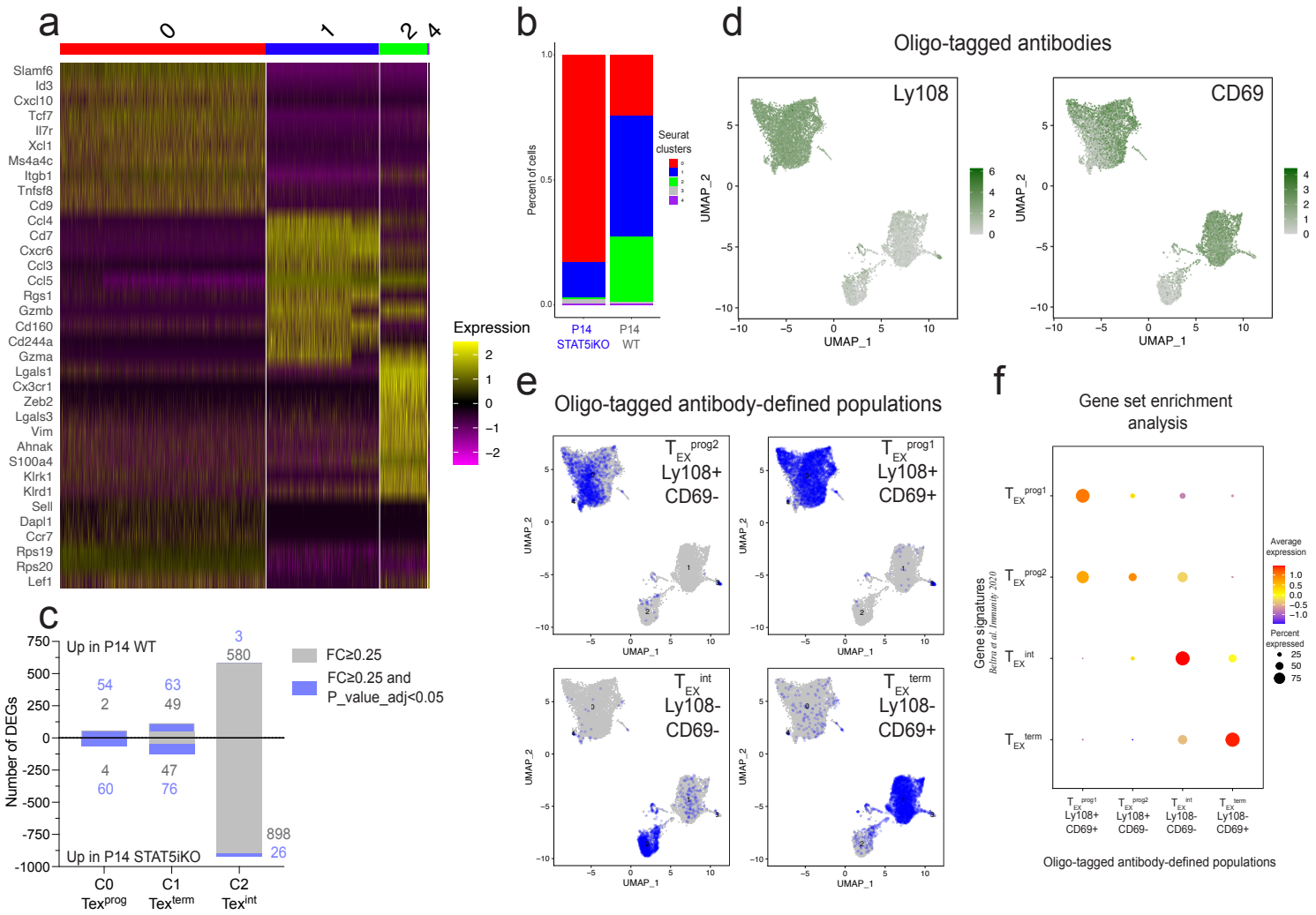

Figure S7

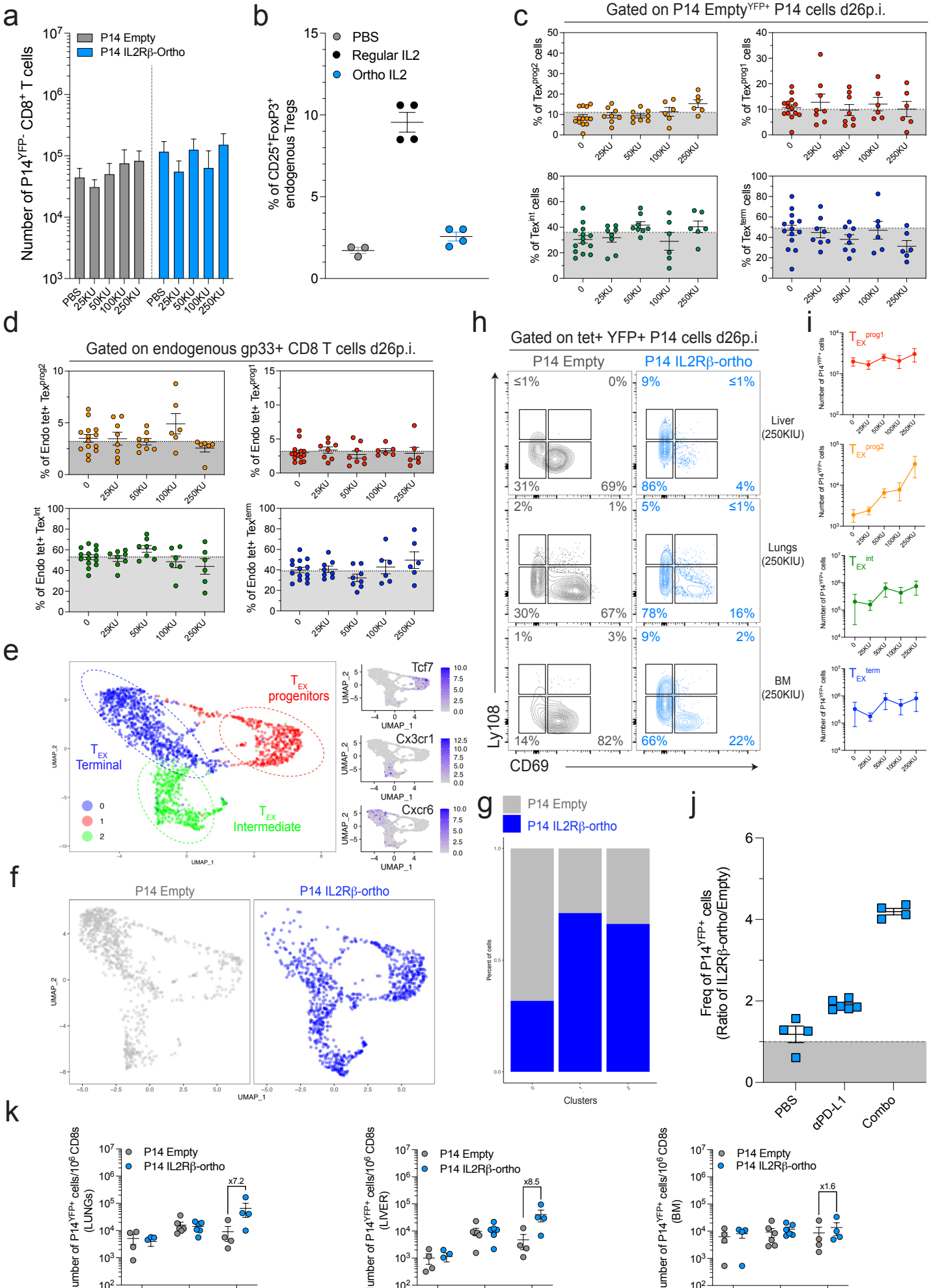

Figure. S8